# We are IntechOpen, the world's leading publisher of Open Access books Built by scientists, for scientists

**4,800**
Open access books available

**122,000**
International authors and editors

**135M**
Downloads

Our authors are among the

**154**
Countries delivered to

**TOP 1%**
most cited scientists

**12.2%**
Contributors from top 500 universities


WEB OF SCIENCE™

Selection of our books indexed in the Book Citation Index in Web of Science™ Core Collection (BKCI)

## Interested in publishing with us?
## Contact book.department@intechopen.com

Numbers displayed above are based on latest data collected.
For more information visit www.intechopen.com

# 9

# The Nature of Electromagnetic Waves in Metamaterials and Metamaterial-inspired Configurations

Rui Yang[1,2] and Yongjun Xie[1]
[1] *National Laboratory of Antennas and Microwave Technology, Xidian University, Xi'an, 710071,*
[2] *Department of Electronic Engineering Queen Mary College, University of London, London E1 4NS,*
[1]*China.*
[2]*UK*

## 1. Introduction

Metamaterials possessing various peculiar features have recently attracted an increasing amount of attention in the electromagnetics community. Their unexpected properties have opened up a number of different research directions that are geared towards the enhancement of the performance of microwave components, and overcoming current limitations. In this Chapter, the fundamental model properties of metamaterials and metamaterial based structures are demonstrated to study the renovated wave propagation.

## 2. Causality in the resonance behavior of metamaterials

Great of interest has been devoted to split ring resonator (SRR) which composes the essential part of left-handed materials [1-3]. Inherently bianisotropic, SRR metamaterials can be obtained by doping a host isotropic medium with two concentric rings separated by a gap, both having splits at opposite sides. As a result, besides the electric and magnetic coupling, the incident field also induces the magnetoelectric coupling [4,5]. Therefore, this kind of artificial magnetic media needs a careful control of the SRR orientation relative to the incident wave as well as the SRR design. Otherwise, the electromagnetic response is significantly more complicated. Smith et al. explored the electromagnetic characterization of the symmetric and asymmetric SRR plane [6]. Vasundara et al. presented the effects of gap orientation on the properties of SRR metamaterials with measured scattering parameters [7]. Aydin et al. investigated the influence of periodicity, misalignment, and disorder on the magnetic resonance gap of SRRs [8]. Gay-Balmaz et al. studied experimentally and numerically the electromagnetic resonances in individual and coupled SRRs [9]. Katsarakis et al. discovered the electric coupling to the magnetic resonance of SRRs under certain orientation [10]. Correspondingly, several analysis modals are employed to unravel the resonance property in the SRR transmission spectra, such as the physical intuition initiated by Pendry et al. [11], lumped element equivalent circuit model proposed by Martin et al.

Source: Wave Propagation in Materials for Modern Applications, Book edited by: Andrey Petrin,
ISBN 978-953-7619-65-7, pp. 526, January 2010, INTECH, Croatia, downloaded from SCIYO.COM

[12], and improved by Aznar et al. [13]. Meanwhile, lots of numerical simulations as well as experimental verifications are carried out for the metamaterial design [14-16]. Especially, Simovski et al. clarified the physical meaning of local constitutive parameters of metamaterials [17], and discussed Bloch material parameters of magneto-dielectric metamaterials [18].

A rigorous full wave analysis of bianisotropic SRR metamaterials is presented here for different electromagnetic field polarization and propagation directions. An alternative physical explanation is gained by revealing the fact that imaginary wave number leads to the SRR resonance. The field distribution over SRRs is then expanded into Floquet modes [19,20] to examine the transmission properties through metamaterials under arbitrary incident waves. Evanescent Floquet modes are proved to engender the resonance behavior which accords with the full wave analysis.

### 2.1 Full wave analysis of the SRR metamterials

To account for the magnetoelectric coupling in Maxwell's equations, SRR metamaterials can be described by the constitutive relations [21]

$$\boldsymbol{D} = \varepsilon_0(\bar{\varepsilon} \cdot \boldsymbol{E} + Z_0 \bar{\kappa} \cdot \boldsymbol{H}) \tag{1a}$$

$$\boldsymbol{B} = \mu_0(-\frac{1}{Z_0}\bar{\kappa}^T \cdot \boldsymbol{E} + \bar{\mu} \cdot \boldsymbol{H}) \tag{1b}$$

where $Z_0 = \sqrt{\mu_0/\varepsilon_0}$ , $\bar{\varepsilon}$ and $\bar{\mu}$ are the relative electric permittivity and relative magnetic permeability tensors, $\bar{\kappa}$ is the magnetoelectric coupling dimensionless tensor.

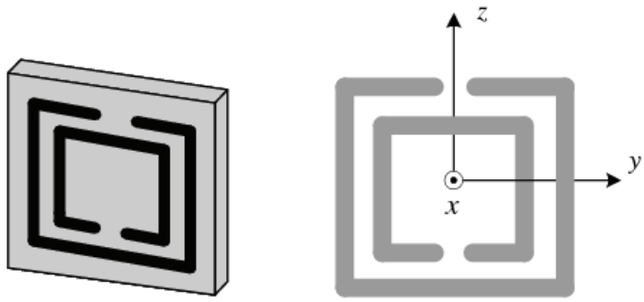


Fig. 1. The SRR unit cell

For axes fixed to the SRR as shown in Fig. 1, only certain components of $\bar{\varepsilon}$ , $\bar{\mu}$ and $\bar{\kappa}$ tensors are of significance without losses [4,5]

$$\varepsilon_{xx} = 1 \text{ , } \varepsilon_{yy} = a + \frac{b\omega^2}{(\omega_0^2 - \omega^2)} \text{ , } \varepsilon_{zz} = a \tag{2a}$$

$$\mu_{xx} = 1 + \frac{c\omega^2}{(\omega_0^2 - \omega^2)} \text{ , } \mu_{yy} = 1 \text{ , } \mu_{zz} = 1 \tag{2b}$$

$$\kappa_{yx} = -i\kappa = -\frac{id\omega_0\omega}{(\omega_0^2 - \omega^2)} \tag{2c}$$

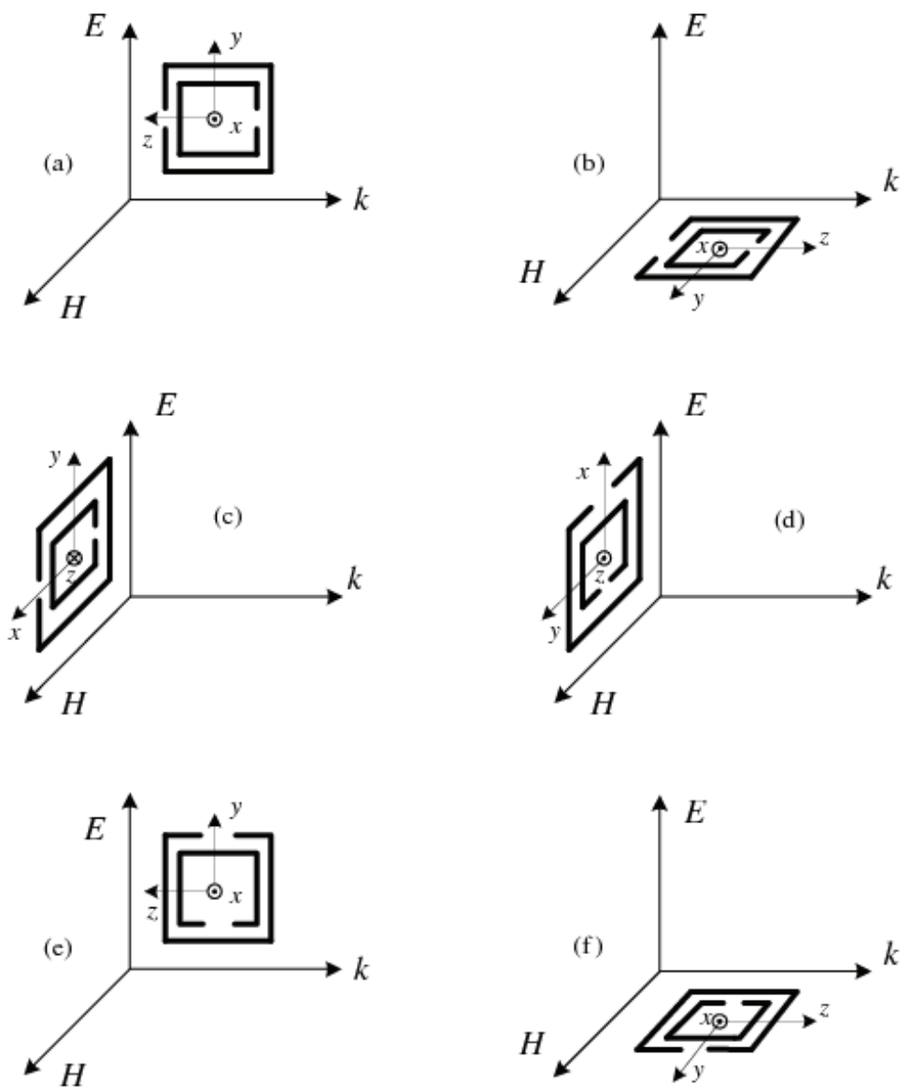


Fig. 2. Six orientations of SRR relative to different electromagnetic field polarization and propagation direction

$\omega_0$ is the resonance frequency, and *a*, *b*, *c*, *d* in Fig. 1 are related to the geometry of the SRR. For other SRR orientations, the $\bar{\varepsilon}$ , $\bar{\mu}$ and $\bar{\kappa}$ tensors just need a coordinates transformation. Introducing a normalized magnetic field $\boldsymbol{h} = Z_0 \boldsymbol{H}$ , from Maxwell's curl equation for source free regions together with (1), (2), one may write

$$-\mathrm{i}\nabla' \times \mathbf{h} = \bar{\varepsilon} \cdot \mathbf{E} + \bar{\kappa} \cdot \mathbf{h} \tag{3a}$$

$$\mathrm{i}\nabla' \times \mathbf{E} = -\bar{\kappa}^T \cdot \mathbf{E} + \bar{\mu} \cdot \mathbf{h} \tag{3b}$$

where $\nabla' = \nabla / k_0$ .

For the case in Fig. 2a, where magnetic field ***H*** is perpendicular to the SRR plane and incident ***E*** is parallel to the gapbearing sides of SRR. One obtains

$$(\kappa_{yx} + \beta)h_x = -\varepsilon_{yy}E_y \tag{4a}$$

$$(\kappa_{yx} - \beta)E_y = \mu_{xx}h_x \tag{4b}$$

The normalized wave number of the TEM wave satisfies

$$\beta^2 = \mu_{xx}\varepsilon_{yy} + \kappa_{yx}^2 \tag{5}$$

Ref. [4] concluded the same results by considering the bianisotropy role in SRR metamaterials. At given frequency $\omega$, only those modes having $\mu_{xx}\varepsilon_{yy} + \kappa_{yx}^2 > 0$ will propagate. Those modes with $\mu_{xx}\varepsilon_{yy} + \kappa_{yx}^2 < 0$ will lead to an imaginary $\beta$, meaning that all field components will decay exponentially away from the source of excitation. Since $\kappa_{yx}^2 < 0$, this SRR orientation will achieve the resonance stop band when the constitutive parameters are single negative, including $\varepsilon_{yy} > 0$, $\mu_{xx} < 0$ case, as well as $\varepsilon_{yy} < 0$, $\mu_{xx} > 0$ case. When the constitutive parameters are double negative or double positive with the condition $\left|\mu_{xx}\varepsilon_{yy}\right| < \left|\kappa_{yx}^2\right|$, the resonance stop band will also occur.

For the case in Fig. 2b, where incident ***E*** is perpendicular to the SRR plane, and magnetic field ***H*** is parallel to the gapbearing sides of SRR, one obtains

$$\beta h_y = \varepsilon_{xx}E_x \tag{6a}$$

$$\beta E_x = \mu_{yy}h_y \tag{6b}$$

The normalized wave number satisfies

$$\beta^2 = \varepsilon_{xx}\mu_{yy} = 1 \tag{7}$$

which indicates that metamaterials with this SRR orientation has little influence to do with TEM waves of such electromagnetic field polarization and propagation direction. Meanwhile, there is no resonance stop band.

Through the similar analysis, metamaterials with the six SRR orientations can be re-categorized into three groups according to Maxwell's equations. The ones shown in Fig. 2a, 2b are one group, so do those in Fig. 2c, 2d, as well as those in Fig. 2e, 2f. The wave numbers for the other four cases are listed in Table 1. The case in Fig. 2c has been studied in Ref. [10],

| SRR orientation | Fig. 2c | Fig. 2d | Fig. 2e | Fig. 2f |
|---|---|---|---|---|
| $\beta^2$ | $\varepsilon_{yy}\mu_{xx}$ | $\varepsilon_{xx}\mu_{yy}$ | $\varepsilon_{yy}\mu_{xx}$ | $\varepsilon_{xx}\mu_{yy}$ |
| $\varepsilon$ | $\varepsilon_{yy} = a + \frac{b\omega^2}{(\omega_0^2 - \omega^2)}$ | $\varepsilon_{xx} = a$ | $\varepsilon_{yy} = a$ | $\varepsilon_{xx} = 1$ |
| $\mu$ | $\mu_{xx} = 1$ | $\mu_{yy} = 1$ | $\mu_{xx} = 1 + \frac{c\omega_0^2}{(\omega_0^2 - \omega^2)}$ | $\mu_{yy} = 1$ |

Table 1. Wave numbers for the SRR metamaterials shown in Fig2. c ~ Fig2. f.

where the authors identified the SRR with its outer ring at low frequencies, and illustrated the simulated currents to explain the resonance phenomenon. Here we can see it more clearly that $\varepsilon_{yy}$ becomes less than zero when frequency $\omega$ is larger than the resonance frequency $\omega_0$, leading to the imaginary wave number $\beta$, thus the resonance stop band is achieved. Also Fig. 2e case has the chance to become resonance when $\mu_{xx} < 0$, and there is no resonance stop band for the Fig. 2d and Fig. 2f case.
From the analysis above we can easily conclude that imaginary wave number actually leads to the SRR resonance. Such result has been noted by Simovski *et al.* in their previous work when studied the metamaterial parameters [17,18]. Here we provide an alternative means of characterizing the resonance of SRR metamaterials.

### 2.2 Floquet modes analysis of the SRR metamterials

Consider an electromagnetic wave to be incident on the SRR metamaterial plane with each element distributed periodically along $\hat{x}$ and $\hat{y}$ direction as shown in Fig. 3.

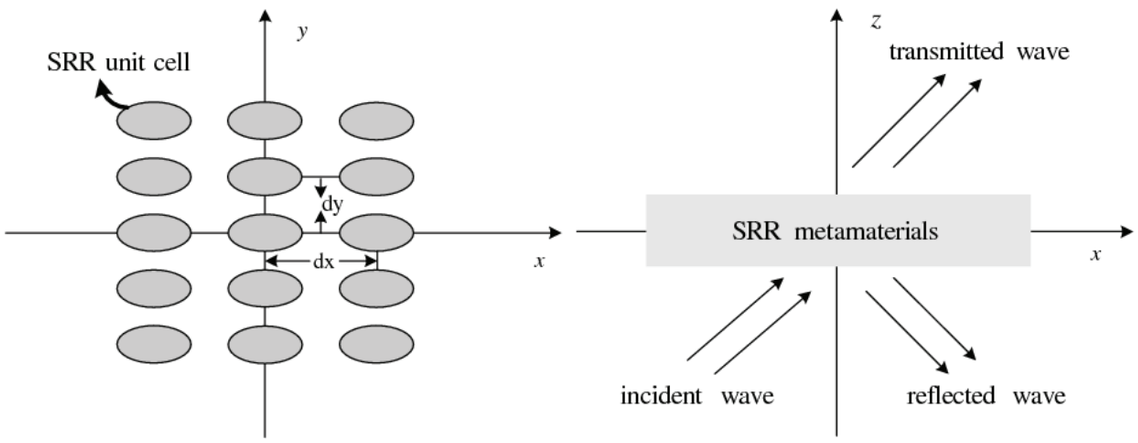


(a) (b)

Fig. 3. Geometry of SRR metamterial plane with incident plane wave (a) Front view (b) Side view

The electromagnetic fields near the SRR elements must satisfy the periodicity requirements imposed by Floquet's theorem. Thus the scattered and the transmitted fields can be expanded as [20]

$$\boldsymbol{E}_{S(T)} = \sum_{m=1}^{2} \sum_{p=-\infty}^{+\infty} \sum_{q=-\infty}^{+\infty} R_{mpq}(B_{mpq}) \boldsymbol{\Psi}_{mpq} \tag{8}$$

where $R_{mpq}$ and $B_{mpq}$ stand for the reflection and the transmission coefficients respectively. The TE and TM vector mode functions $\boldsymbol{\psi}_{mpq}$ can be written as

$$\boldsymbol{\psi}_{1pq} = \frac{1}{(d_x d_y)^{1/2}} \left( \frac{v_{pq}}{t_{pq}} \hat{x} - \frac{u_{pq}}{t_{pq}} \hat{y} \right) \varphi_{pq} \qquad \text{TE-Floquet mode} \tag{9a}$$

$$\boldsymbol{\psi}_{2pq} = \frac{1}{(d_x d_y)^{1/2}}\left(\frac{u_{pq}}{t_{pq}}\hat{\boldsymbol{x}} + \frac{v_{pq}}{t_{pq}}\hat{\boldsymbol{y}}\right)\varphi_{pq} \qquad \text{TM-Floquet mode} \tag{9b}$$

The dominant modes have $p = q = 0$ and the higher order modes have $p \neq 0$ or $q \neq 0$. And

$$\varphi_{pq} = \exp(-i(u_{pq}\hat{\boldsymbol{x}} + v_{pq}\hat{\boldsymbol{y}} + \gamma_{pq}\hat{\boldsymbol{z}})) \tag{10}$$

Suppose the incidence wave in the direction of $(\theta, \phi)$ with the wave number $k$, one has

$$u_{pq} = k\sin\theta\cos\phi + 2\pi p / d_x \tag{11a}$$

$$v_{pq} = k\sin\theta\sin\phi + 2\pi q / d_y \tag{11b}$$

$$\begin{aligned} \gamma_{pq} &= (k^2 - t_{pq}^2)^{1/2}, && \text{for } k^2 > t_{pq}^2 \\ &= -i\left|(k^2 - t_{pq}^2)^{1/2}\right| && \text{for } k^2 < t_{pq}^2 \end{aligned} \tag{11c}$$

with

$$t_{pq}^2 = u_{pq}^2 + v_{pq}^2 \tag{12}$$

It is known that a homogenous electromagnetic wave can always be decomposed into a combination of two plane waves with E-field perpendicular or parallel to the incident plane corresponding to the TE- and TM-Floquet modes. Therefore, the effects of any incident wave of either polarization at arbitrary angle $(\theta, \phi)$ will be easily examined for the SRR resonance behavior.

The modal propagation constant $\gamma_{pq}$ is positive real for the propagating modes and is negative imaginary for the evanescent modes. Since the resonance of SRR metamaterials is often manifested by a dip in the transmitted curves, let's see the $S$ parameters for the SRR metamaterial plane.

$$S_{11}^{mpq} = \frac{R_{mpq}(1 - T_{pq}^2)}{1 - R_{mpq}^2 T_{pq}^2},\ S_{21}^{mpq} = \frac{T_{pq}(1 - R_{mpq}^2)}{1 - R_{mpq}^2 T_{pq}^2} \tag{13}$$

with the reflection coefficients $\left|R_{mpq}\right| \leq 1$ and propagation factor $T_{pq} = \exp(-i\gamma_{pq} z)$. Apparently, $S_{21}$ decreases while $T_{pq}$ gets smaller. When $\gamma_{pq}$ becomes pure imaginary, all the field components will decay exponentially from the source of excitation, leading to the dip in transmitted ($S_{21}$) curves. This reveals the fact that evanescent Floquet modes actually engender the resonance behavior which exactly accords with the full wave analysis.

Consider the SRR metamaterials with the orientation in Fig. 2a, the dimensions of the SRR defined in (2) are $a = 0.84$ mm, $b = 1.17$ mm, $c = d = 0.33$ mm, and the dielectric substrate with $\varepsilon_r = 4.8$ is 1.6 mm thick. The SRR metamaterial plane is 3.63 mm in $\hat{\boldsymbol{z}}$ direction with element period $dx = 5.6$ mm, $dy = 5$ mm along $\hat{\boldsymbol{x}}$ and $\hat{\boldsymbol{y}}$ direction. Fig. 4 shows the resonance behavior for a plane wave incident in the XoZ plane ($\phi = 0^\circ$). With E field perpendicular to the incident plane, the resonance only happens in the TE-Floquet modes.

The resonant frequency $8.2\ \mathrm{GHz}$ hardly changes, while the resonance intensity is sensitive to the incident angle. One knows that an H component perpendicular to the SRR plane will induce a circular current flow inside the SRRs, which in turn produces just above the resonance frequency a large magnetic dipole moment antiparallel to $H_{\perp} = H\cos\theta$, leading to a negative $\mu$. As the SRR orientation shown in Fig. 2a, the E-field parallel to the gap bearing also introduces the electric resonance, thus the SRR resonance behavior becomes more complicated as the variation of incident angle. As shown in Fig. 4a, when $\theta = 40^{\circ}$, the resonance intensity is of most significance. When $\theta = 0^{\circ}$ and $\theta = 20^{\circ}$, one obtains the almost equal resonance intensity. When $\theta = 60^{\circ}$, the resonance is much weaker. In addition, the bandwidth increases a little as the incidence angle increases. The phases of $S_{11}$ and $S_{21}$ for the SRR metamaterials are given in Fig. 4b. When $\theta = 0^{\circ}$, one finds that the phase of $S_{11}$ goes to zero and $S_{21}$ has an extremely sharp change at the resonance point, which makes the metamaterials can be characterized as a magnetic conductor in this region. However, this does not hold true for the most significant resonance intensity when $\theta = 40^{\circ}$, since it is not merely engendered by H component.

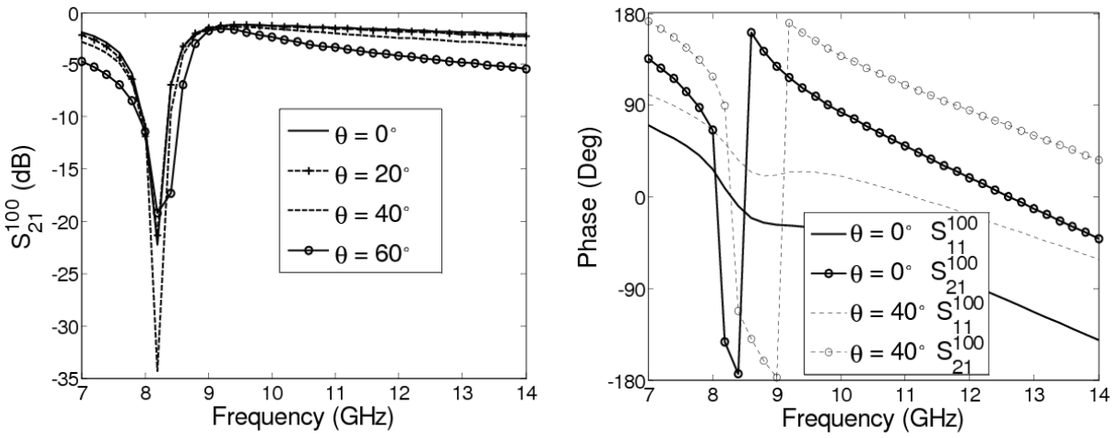


(a) (b)

Fig. 4. Transmitted TE-Floquet modes for the SRR metamaterials with the orientation in Fig. 2a (a) magnitudes (b) phases

The graph in Fig. 5 shows the resonance behavior for a plane wave incident in the YoZ plane ($\phi = 90^{\circ}$). With E-field parallel to the incident plane, the resonant behavior this time only happens in the TM-Floquet modes. Similar to the resonance behavior in Fig. 4a, the resonance frequency $8.2\ \mathrm{GHz}$ stays the same but the resonance intensity changes with the incidence angle. When $\theta = 60^{\circ}$, the resonance intensity is of most significance. When $\theta = 20^{\circ}$ and $\theta = 40^{\circ}$, one obtains the almost equal and weakest resonance. The intermediate resonance intensity is obtained when $\theta = 0^{\circ}$. The bandwidth decreases a little as the incidence angle increases. In Fig. 5b the phases of $S$ parameters are illustrated. One finds that metamaterials can still be characterized as a magnetic conductor when $\theta = 0^{\circ}$, while the phase of $S_{11}$ and $S_{21}$ are more complex when $\theta = 60^{\circ}$.

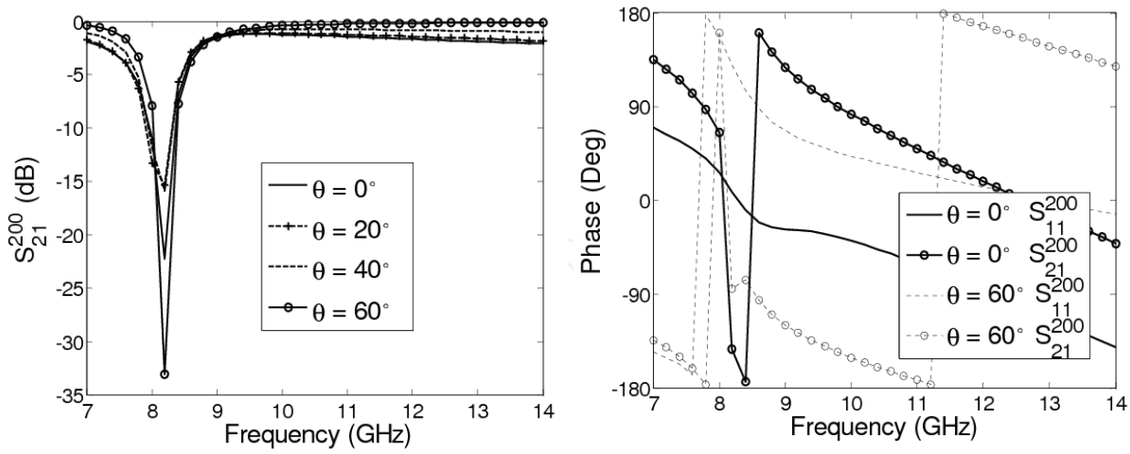


(a) (b)

Fig. 5. Transmitted TM-Floquet modes for the SRR metamaterials with the orientation in Fig. 2a (a) magnitudes (b) phases

Table 2 demonstrates the transmission factor for TE- and TM-Floquet modes at the resonance frequency 8.2 GHz . As is shown, $|T|$ turns smaller when the resonance intensity becomes more significant. And it is the fact that $|T|$ turns smaller because the evanescent modes play more important role, therefore one can conclude that metamaterial resonance is engendered by the evanescent Floquet modes.

| | | | |
|---|---|---|---|
| TE-Floquet mode $\phi = 0^\circ$ | $\theta = 0^\circ$ | $S_{11}^{100} = -0.4117 + \mathrm{i}(-0.9080)$<br>$S_{21}^{100} = -0.0614 + \mathrm{i}(-0.0466)$ | $\lvert T\rvert = 0.0424$ |
| | $\theta = 40^\circ$ | $S_{11}^{100} = 0.7535 + \mathrm{i}(-0.6571)$<br>$S_{21}^{100} = 0.0001 + \mathrm{i}(0.0193)$ | $\lvert T\rvert = 0.0147$ |
| TM-Floquet mode $\phi = 90^\circ$ | $\theta = 0^\circ$ | $S_{11}^{200} = -0.4117 + \mathrm{i}(-0.9080)$<br>$S_{21}^{200} = -0.0614 + \mathrm{i}(-0.0466)$ | $\lvert T\rvert = 0.0424$ |
| | $\theta = 60^\circ$ | $S_{11}^{200} = 0.6596 + \mathrm{i}(-0.8780)$<br>$S_{21}^{200} = 0.0019 + \mathrm{i}(-0.0222)$ | $\lvert T\rvert = 0.0126$ |

Table 2. Transmission factor for TE- and TM-Floquet modes at the resonance frequency 8.2 GHz

For the other two resonance cases in Fig. 2c (1.6 mm thick in $\hat{z}$ direction with $dx = 3.63$mm , $dy = 5$ mm ) and Fig. 2e ( 5 mm thick in $\hat{z}$ direction with $dx = 5.6$ mm , $dy = 3.63$ mm ), Fig. 6 shows the resonance behavior for a plane wave incident in the XoZ plane ( $\phi = 0^\circ$ ) and similar results hold true for the wave incident in the YoZ plane ( $\phi = 90^\circ$ ). The electric resonance for Fig. 2c case shown in Fig. 6a has the most significance resonance intensity when $\theta = 30^\circ$ at 8.6 GHz . On the other hand, the magnetic resonance for Fig. 2e case shown in Fig. 6b demonstrates the general downward trend with the incident angle 8.8 GHz , which has its most significant intensity when $\theta = 0^\circ$ , and weakest when $\theta = 60^\circ$ .

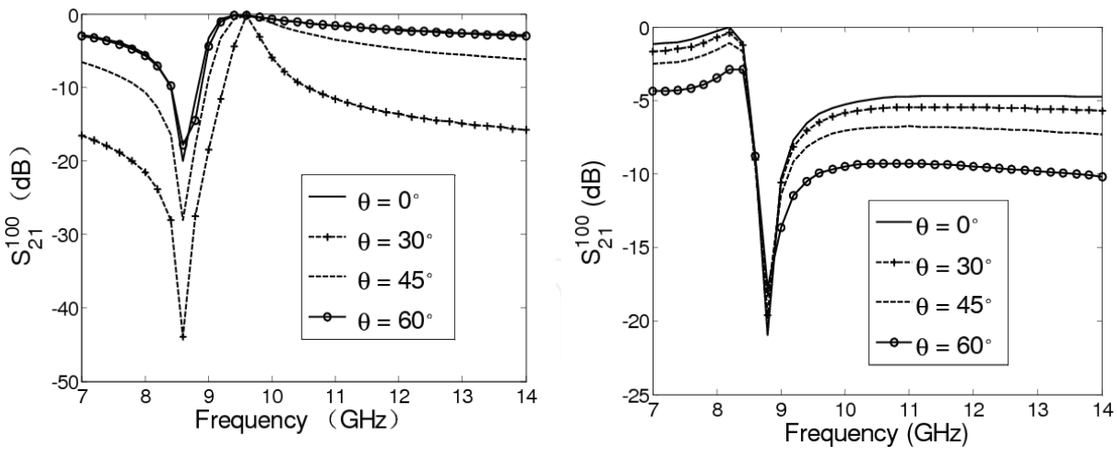


(a) (b)

Fig. 6. Transmitted TE-Floquet modes for the SRR metamaterials with (a) the orientation in Fig. 2c (b) the orientation in Fig. 2e

## 3. Propagation features of waveguides structures with SRR metamaterials

Waveguiding structures based on metamaterial media have recently been considered by several research groups showing how the presence of one or both negative constitutive parameters may give rise to unexpected and interesting propagation properties [22]-[29]. The absence of fundamental mode and sign-varying energy flux in the negative refractive index waveguide are revealed [25]. Rectangular waveguide filled with anisotropic single negative metamaterials are shown to support backward-wave propagation [26]. Moreover, Results for isotropic double negative metamaterial H waveguides are reported, including backward propagation, mode bifurcation and coupling effects [27]. The use of single negative metamaterials as the embedding medium for nonradiative dielectric (NRD) waveguides is examined [28]. Unimodal surface wave propagation in metamaterial NRD waveguides is obtained [29]. However, the presented literatures almost focus on the negative effects of both permittivity and permeability to the metamaterial based waveguides, whereas magnetoelectric coupling of the bianisotropic effects may lead to more dramatically unexpected features in the waveguiding structures.

With the consideration above, metamaterial loaded waveguiding structures are investigated to explore the different dispersion properties of guided waves. It is shown that transverse magnetic and transverse electric waves with non-cutoff frequency and enhanced bandwidth become into existence under certain circumstances in metamaterial parallel plate waveguide and rectangular waveguide. When doping uniaxial bianisotropic SRR metamaterials into NRD waveguides and H waveguides, both longitudinal-section magnetic (LSM) and longitudinal-section electric (LSE) waves are capable of propagating very slowly due to metamaterial bianisotropic effects. Particularly, some abnormal higher-order LSM and LSE modes with negative slope of the phase constant versus frequency may appear when metamaterials are double negative. Such modes will eventually lead to the leakage. Fortunately, for other modes, leakage can be reduced due to the magnetoelectric coupling. Particularly, when the metamaterials are of single negative parameters, leakage elimination can be achieved.

### 3.1 Parallel plate waveguides and rectangular waveguides

Geometry of parallel plate waveguide and rectangular waveguides filled with SRR metamaterials are shown in Fig. 7. The strip width $W$ in Fig. 7(a) is assumed to be much greater than the separation $l$ between the two plates, so that fringing fields and any $x$-variation can be ignored. And it is standard convention to have the longest side of the rectangular waveguide along the $x$ -axis, so that $u > v$ in Fig. 7(b).

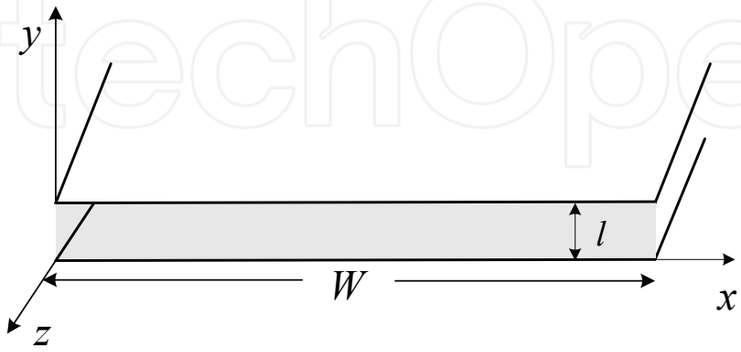


(a)

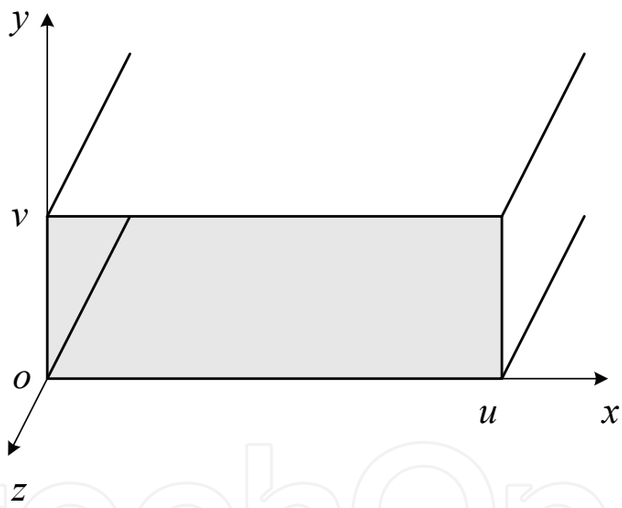


(b)

Fig. 7. Geometry of parallel plate waveguide and rectangular waveguide filled with SRR metamaterials

According to Fig. 2, metamaterial waveguide with different SRR orientations are illustrated in Fig. 8. For Fig. 8(a), one can express the following coupled equations for the longitudinal fields:

$$\begin{aligned}&\left(\frac{\varepsilon_{xx}}{\beta^2-\varepsilon_{xx}\mu_{yy}}\partial^2_{x'}+\frac{\varepsilon_{yy}}{\beta^2-\mu_{xx}\varepsilon_{yy}+\kappa^2}\partial^2_{y'}-\varepsilon_{zz}\right)E_z\\&\qquad=\left(\frac{-\beta}{\beta^2-\varepsilon_{xx}\mu_{yy}}+\frac{\beta-i\kappa}{\beta^2-\mu_{xx}\varepsilon_{yy}+\kappa^2}\right)\partial^2_{x'y'}h_z\end{aligned} \tag{14a}$$

$$\begin{aligned}&(\frac{\mu_{xx}}{\beta^2-\mu_{xx}\varepsilon_{yy}+\kappa^2}\partial^2_{x'}+\frac{\mu_{yy}}{\beta^2-\varepsilon_{xx}\mu_{yy}}\partial^2_{y'}-\mu_{zz})h_z\\&\qquad=(\frac{-\beta}{\beta^2-\varepsilon_{xx}\mu_{yy}}+\frac{\beta-i\kappa}{\beta^2-\mu_{xx}\varepsilon_{yy}+\kappa^2})\partial^2_{x'y'}E_z\end{aligned} \tag{14b}$$

### 3.1.1 Non-cutoff frequency modes

For the parallel plate waveguides, TM waves are characterized by $h_z=0$ and a nonzero $E_z$ field which satisfies the reduced wave Eq. (14a), with $\partial x'=0$ ,

$$[\partial^2_{y'}+\frac{\varepsilon_{zz}}{\varepsilon_{yy}}(\mu_{xx}\varepsilon_{yy}-\kappa^2-\beta^2)]E_z=0 \tag{15}$$

where

$$k_z^2=\beta^2k_0^2=(\mu_{xx}\varepsilon_{yy}-\kappa^2)k_0^2-\frac{\varepsilon_{yy}}{\varepsilon_{zz}}k_c^2 \tag{16}$$

and $k_c=\frac{n\pi}{l}$, ( $n=0,1,2\cdots$ ) is the cutoff wave number constrained to discrete values.

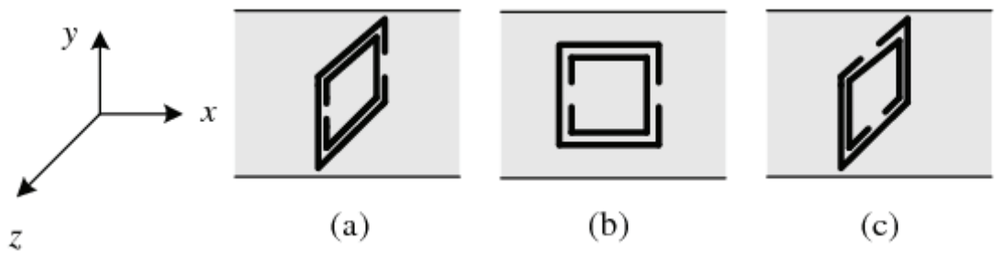


Fig. 8. Metamaterial waveguide with different SRR orientations

Observe that for $n=0$ , the $TM_0$ mode is actually identical to the TEM mode shown in Fig. 2(a), therefore, this $TM_0$ mode has a cutoff phenomenon while SRR resonance. However, from (16) one knows that TM mode has the chance to propagate with no cutoff frequency when $\varepsilon_{yy}<0$ and $\mu_{xx}\varepsilon_{yy}-\kappa^2>0$ , as shown in Fig. 9. Similar results hold true for the TE modes in Fig. 8(b), and TM modes in Fig. 8(c), which are corresponding to the resonance cases in the Fig. 2.

For the rectangular waveguides, one can see that if $\kappa\neq0$ , decoupling of $E_z$ and $h_z$ occurs only when $\partial_{x'}\equiv0$ or $\partial_{y'}\equiv0$ , therefore we only consider $TE_{mn}$ modes with $m=0$ or $n=0$ , since neither *m* nor *n* can be zero for TM modes in a rectangular waveguide. When $\partial_{y'}\equiv0$ , one has the following decoupled equation and boundary condition for $TE_{m0}$ modes from Eq. (14b)

$$(\partial^2_{x'}-\frac{\beta^2-\mu_{xx}\varepsilon_{yy}+\kappa^2}{\mu_{xx}}\mu_{zz})h_z=0 \tag{17}$$

where

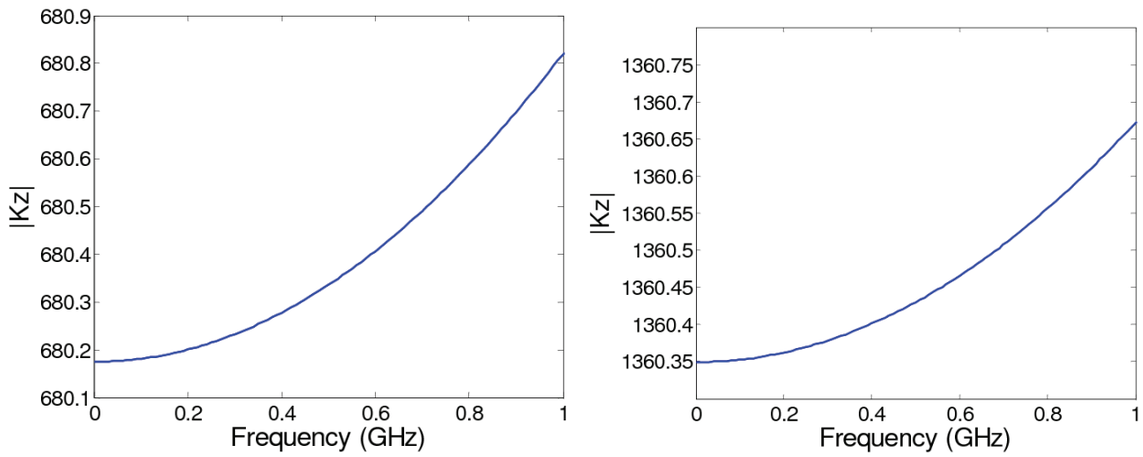


(a) $TM_1$ (b) $TM_2$

Fig. 9. The none cutoff frequency TM modes in parallel plate waveguide with SRR metamaterials $\varepsilon_{yy} = -3$, $\varepsilon_{zz} = 1$, $\mu_{xx} = -1$, $\kappa = 1$, $l = 8$ mm

$$k_z^2 = \beta^2 k_0^2 = (\mu_{xx}\varepsilon_{yy} - \kappa^2)k_0^2 - \frac{\mu_{xx}}{\mu_{zz}}k_c^2 \tag{18}$$

Akin to the modes in the parallel plate waveguide, none-cutoff frequency modes also exist under certain condition.

### 3.1.2 Enhanced bandwidth of single mode operation

For the parallel plate waveguides, the TE modes in Fig. 8(a), characterized by $E_z = 0$ and a nonzero $h_z$ field which satisfies the reduced wave Eq. (14b), with $\partial x' = 0$. Through the similar derivation, one can obtain

$$f_c = \frac{nc}{2l} \qquad (n \geq 1) \tag{19}$$

The TM modes in Fig. 8(b), and TE modes in Fig. 8(c) corresponding to the non-resonance cases in the Fig. 2 achieve the identical cutoff frequencies $f_c = \frac{nc}{2l}$, which is the maximum value for ordinary TM and TE waves, promising a bandwidth enhancement for single-mode operation in material containing waveguide.

For the rectangular waveguides, one can see that $TE_{0n}$ modes in Fig. 8(a) and Fig. 8(c) achieve the cutoff frequency of $f_c = \frac{nc}{2v}$, $TE_{m0}$ modes in Fig. 8(b) obtains the cutoff frequency of $f_c = \frac{nc}{2u}$, which are equal to the ones of air containing rectangular waveguide, promising a bandwidth enhancement for single-mode operation in material containing waveguide.

### 3.2 Nonradiative dielectric waveguides and H waveguides

Consider the particular case of SRR metamaterials where two sets of SRR microstructures with different orientations are included in NRD waveguides and H waveguides as shown in Fig. 10.

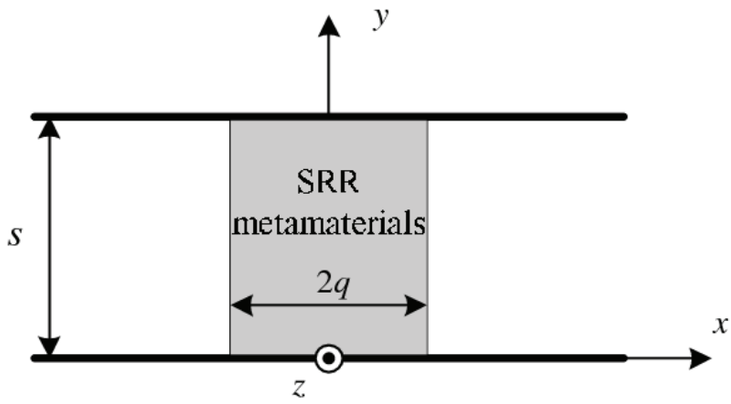


Fig. 10. Configuration of NRD waveguide and H waveguide with SRR metamaterials

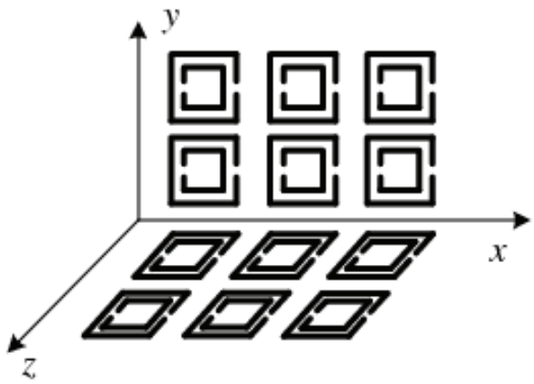


Fig. 11. Spatial orientation of SRRs in the host isotropic medium

The relative orientation of these two ensembles is in Fig. 11 and the $\bar{\varepsilon}$ , $\bar{\mu}$ and $\bar{\kappa}$ tensors in Eq. (1) have the following uniaxial form [30]

$$\bar{\varepsilon} = \begin{bmatrix} \varepsilon_1 & 0 & 0 \\ 0 & \varepsilon_2 & 0 \\ 0 & 0 & \varepsilon_2 \end{bmatrix}, \bar{\mu} = \begin{bmatrix} \mu_1 & 0 & 0 \\ 0 & \mu_2 & 0 \\ 0 & 0 & \mu_2 \end{bmatrix}, \bar{\kappa} = \mathrm{i} \begin{bmatrix} 0 & 0 & 0 \\ 0 & 0 & \kappa \\ 0 & -\kappa & 0 \end{bmatrix} \tag{20}$$

where

$$\varepsilon_1 \propto a\,,\ \varepsilon_2 \propto 1 + \varsigma \frac{a(\omega_0^2 - \omega^2) + b\omega^2}{(\omega_0^2 - \omega^2)} \tag{21a}$$

$$\mu_1 \propto 1\,,\ \mu_2 \propto \xi + \frac{(\omega_0^2 - \omega^2) + c\omega^2}{(\omega_0^2 - \omega^2)} \tag{21b}$$

$$\kappa \propto \frac{d\omega_0\omega}{(\omega_0^2 - \omega^2)} \tag{21c}$$

$\varsigma$ , $\xi$ reflect the different changes of $\varepsilon$ and $\mu$ components in $\hat{y}\hat{y}$ and $\hat{z}\hat{z}$ direction. Therefore, $\varepsilon_1$ and $\mu_1$ are always positive, whereas $\varepsilon_2$ and $\mu_2$ can be negative in certain frequency band.

For the full wave analysis of the NRD waveguides and H waveguides modal properties, the eigenvalue problem is solved in the complex plane so as to examine the leakage property of H waveguides. The LSM modes are characterized by $h_x = 0$ with nonzero $h_y$ as the supporting field which satisfies

$$\partial_{x'}^2 h_y + \frac{\varepsilon_2}{\varepsilon_1}\partial_{y'}^2 h_y = -(\varepsilon_2\mu_2 - \kappa^2 - \frac{\varepsilon_2}{\varepsilon_1}k_z^{'2})h_y \tag{22}$$

where $k_z^{'} = k_z/k_0 = \beta_z - \mathrm{i}\alpha_z$ is the complex normalized longitudinal wave number. All other field components can be expressed as

$$h_z = -\mathrm{i}\frac{1}{k_z^{'}}\partial_{y'}h_y \tag{23a}$$

$$E_x = -\frac{1}{k_z^{'}\varepsilon_1}(\partial_{y'}^2 h_y - k_z^{'2}h_y) \tag{23b}$$

$$E_y = \frac{1}{k_z^{'}\varepsilon_2}(\partial_{y'}\partial_{x'}h_y - \kappa\partial_{y'}h_y) \tag{23c}$$

$$E_z = -\mathrm{i}\frac{1}{\varepsilon_2}(\partial_{x'}h_y - \kappa h_y) \tag{23d}$$

Express $h_y$ as a product of two separate variable functions in the form

$$h_y = f(x')g(y')\exp(-\mathrm{i}k_z^{'}z') \tag{24}$$

such that

$$\partial_{x'}^2 f(x') + k_x^{'2} f(x') = 0 \tag{25a}$$

$$\partial_{y'}^2 g(y') + k_y^{'2} g(y') = 0 \tag{25b}$$

where $k_x^{'} = k_x / k_0$ and $k_y^{'} = k_y / k_0$ are the complex normalized transverse wave numbers. Substituting back into Eq. (22), the normalized wave numbers can be expressed

$$k_{x1}^{'2} + \frac{\varepsilon_2}{\varepsilon_1}(k_y^{'2} + k_z^{'2}) = \varepsilon_2\mu_2 - \kappa^2 \tag{26a}$$

$$k_{x0}^{'2} + k_y^{'2} + k_z^{'2} = 1 \tag{26b}$$

One has $k_x^{'} = k_{x1}^{'} = \beta_{x1} - \mathrm{i}\alpha_{x1}$ for $|x'| < q'$, while for $|x'| > q'$, one should take $k_x^{'} = k_{x0}^{'} = \beta_{x0} - \mathrm{i}\alpha_{x0}$. Apply the boundary conditions on the perfectly electric conductor planes to other field components, one can write

$$g(y') = G\sin(k_y^{'}y') \qquad (n = 1, 2, 3, \cdots) \tag{27}$$

where $G$ is the amplitude constant, and $k_y^{'} = n\frac{\pi}{s'}$ with $s' = k_0 s$. The $n$ index gives the number of half waves along $y$. And

$$f(x') = \begin{cases} F_1 \exp[k_{x0}^{'}(x'+q')] & x' < -q' \\ F_2[\cos(k_{x1}^{'}x') + R\sin(k_{x1}^{'}x')] & -q' < x < q' \\ F_3 \exp[-k_{x0}^{'}(x'-q')] & q' < x' \end{cases} \tag{28}$$

Enforcing the continuity conditions at both $x' = \pm q'$, the modal equation for the LSM modes can be finally derived

$$[k_{x1}^{'}\cot(k_{x1}^{'}q') + k_{x0}^{'}\varepsilon_2][k_{x1}^{'}\tan(k_{x1}^{'}q') - k_{x0}^{'}\varepsilon_2] + \kappa^2 = 0 \tag{29}$$

the order of eigensolution of Eq. (29) gives the $m$ index ( $m = 0,1,2,\cdots$ ) appearing in $\mathrm{LSM}_{mn}$. From the similar derivation, the LSE modes can be defined as

$$[k_{x1}^{'}\cot(k_{x1}^{'}q') + k_{x0}^{'}\mu_2][k_{x1}^{'}\tan(k_{x1}^{'}q') - k_{x0}^{'}\mu_2] + \kappa^2 = 0 \tag{30}$$

and the normalized transverse wavenumber in the slab should be given by

$$k_{x1}^{'\,2} + \frac{\mu_2}{\mu_1}(k_y^{'\,2} + k_z^{'\,2}) = \varepsilon_2\mu_2 - \kappa^2 \tag{31}$$

instead of Eq. (26a). Hereafter, we only consider the LSM modes, and the following results hold true for the LSE modes.

### 3.2.1 Slow wave propagation

Figure 12(a) presents the operational diagram for LSM modes, the real part of the longitudinal wave number $|\beta_z|$ decreases gradually as the magnetoelectric coupling turns larger in the case that $\varepsilon_2$ and $\mu_2$ are of positive values. Maximum $\kappa$ is achieved under the cutoff condition $k_z^{'} = 0$.

$$|\kappa_{\max}| = \sqrt{\varepsilon_2\mu_2 - \left|\frac{\varepsilon_2}{\varepsilon_1}\right| k_y^{'\,2} - k_{x1}^{'\,2}} \tag{32}$$

Since the guide wavelength defined as $\lambda_g = \frac{2\pi}{\beta_z}$ becomes smaller when longitudinal wave number increases, the corresponding phase velocity $v = T\lambda$ of the modes will be much slower. From Eq. (21), one can see that in the frequency that $\omega$ is far larger than the resonance frequency $\omega_0$, both positive $\varepsilon_2$ and $\mu_2$ as well as smaller absolute value of $\kappa$ can be obtained, thus slow wave propagation will appear.

In Fig. 12(b), one can see that $|\beta_z|$ shows a general upward trend when the magnetoelectric coupling becomes significant in the case that $\varepsilon_2$ and $\mu_2$ are both negative. Minimum value for $\kappa$ with the cutoff condition $k_z^{'} = 0$ can be obtained,

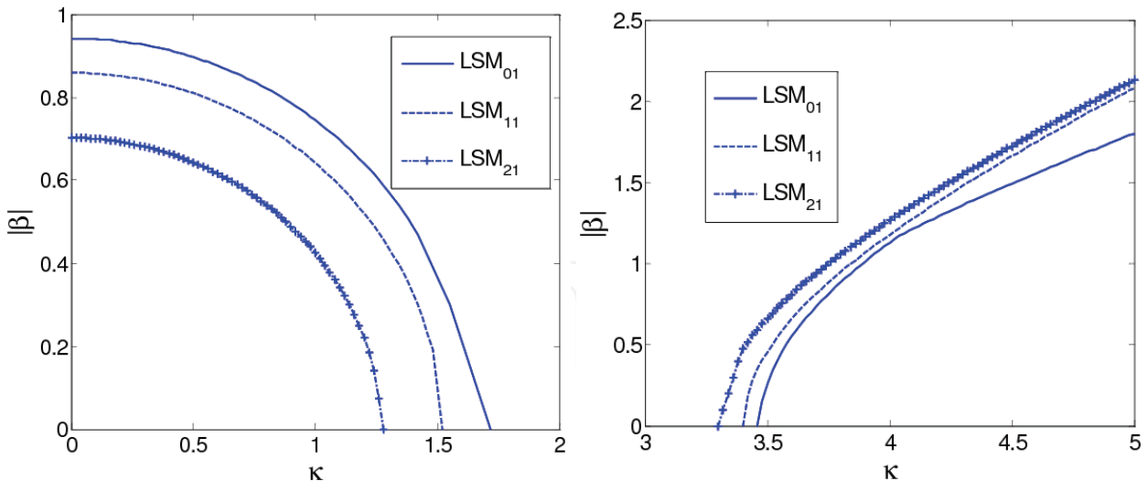


Fig. 12. Relationship of $|\beta_z|$ and magnetoelectric coupling $\kappa$ in nonradiative dielectric waveguide with SRR metamaterials
(a) $\varepsilon_1 = 1$, $\varepsilon_2 = 3$, $\mu_2 = 2.5$, $f = 35$ GHz, $s = 0.4\lambda_0$, $q = 0.6\lambda_0$
(b) $\varepsilon_1 = 1$, $\varepsilon_2 = -3$, $\mu_2 = -2.5$, $f = 35$ GHz, $s = 0.4\lambda_0$, $q = 0.6\lambda_0$

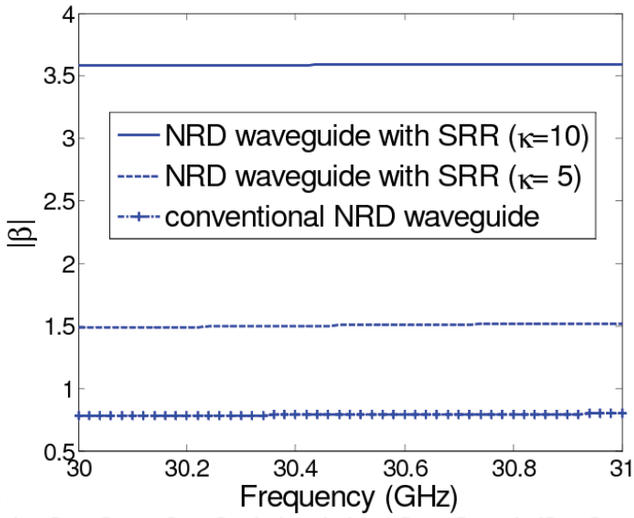


Fig. 13. Variation of the $|\beta_z|$ with frequency $f$ for the dominant $LSM_{01}$ (conventional NRD waveguide with $\varepsilon_r = 4$, $\mu_r = 1$, $s = 4$ mm, $q = 5$ mm; double negative metamaterial NRD waveguide with $\varepsilon_1 = 1$, $\varepsilon_2 = -4$, $\mu_2 = -1$, $\kappa = 5$ and 10, $s = 4$ mm, $q = 5$ mm)

$$|\kappa_{\min}| = \sqrt{\varepsilon_2\mu_2 + \left|\frac{\varepsilon_2}{\varepsilon_1}\right| k_y'^2 - k_{x1}'^2} \tag{33}$$

From Eq. (21), $\varepsilon_2$ and $\mu_2$ have the chance to become negative when $\omega$ is little larger than the resonance frequency $\omega_0$. Meanwhile, the magnetoelectric coupling $\kappa$ has the absolute

value which can be infinitely large within this frequency band. Therefore, the guided waves are able to propagate very slowly, and even approach zero velocity.

Besides, we should stress that when the magnetoelectric coupling vanishes, Eq. (29) and Eq. (30) become a product of two elementary modal equations, which is similar to those of conventional NRD waveguides and H waveguides. Fig. 13 shows that the operational diagram for $LSM_{01}$ modes in a conventional NRD waveguide and a NRD waveguide with SRR metamaterials. Since there exists minimum value for magnetoelectric coupling $\kappa$ in the double negative case, we choose $\kappa = 5$ and $10$ to make sure that $LSM_{01}$ propagates. As can be seen within $[30\ \text{GHz},\ 31\ \text{GHz}]$, the longitudinal wave number of $LSM_{01}$mode in NRD waveguide with SRR metamaterials is always larger than that of the conventional one, thus traveling more slowly, which indicates that NRD waveguide with SRR metamaterials allows more number of wavelength to propagate within the same length, providing feasibility of miniaturization for NRD waveguide.

Let's further consider the power flow of $LSM_{01}$ modes in the NRD waveguide with SRR metamaterials. The time-average power passing a transverse cross-section of the NRD waveguide is

$$\begin{aligned} P_{01} &= \frac{1}{2}\mathrm{Re}\int_{x'=-l'}^{l'}\int_{y'=0}^{s'} E\times h^{*}\cdot\hat{z}dy'dx' \\ &= \pm\frac{1}{2}\mathrm{Re}\int_{x'=-l'}^{l'}\int_{y'=0}^{s'} E_x h_y^{*}dy'dx' \\ &= \pm\frac{F_2^2G^2s'l'}{2\varepsilon_1}[\frac{1}{\beta_z}(\frac{\lambda_0}{2s})+\beta_z] \end{aligned} \tag{34}$$

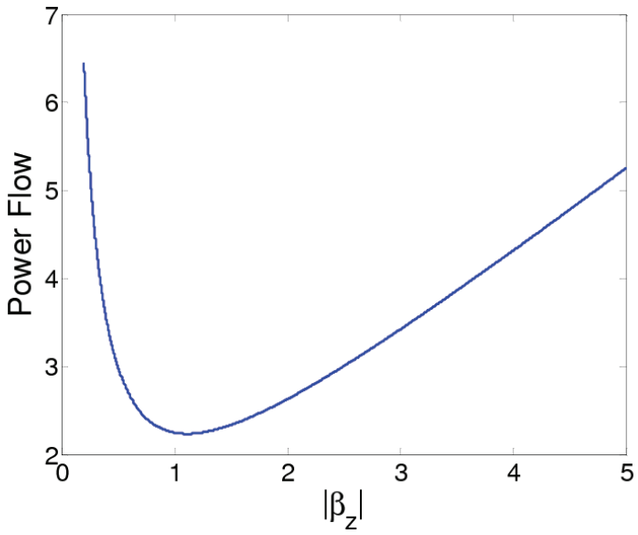


Fig. 14. Energy flow of $LSM_{01}$ mode varied with longitudinal wave number in the NRD waveguide with SRR metamaterials

For $\varepsilon_2$ and $\mu_2$ are both positive, we choose '+', and for the double negative metamaterial case, we choose '-'. As we all know, the double negative metamaterials have the negative wave number, which leads to the positive Poynting vector in Eq. (34). With the choice of

$s = 0.4\lambda_0$, Fig. 14 shows general trend of power flow varied with absolute value of longitudinal wave number by not taking the constant coefficient into account. It can be seen that $P_{01}$ will increase as $|\beta_z|$ becomes larger than $\sqrt{\lambda_0 / 2s} = 1.118$. What is meant by this is that the increasing $|\beta_z|$ will enhance the power flow. From the above analysis, we can discern that metamaterial waveguide with double negative parameters has the chance to achieve infinite large $|\beta_z|$ around the metamaterial resonance frequency. Therefore, inserting metamaterials will strengthen the power flow of the conventional NRD waveguide. It is worth noting that such strengthen trend of power flow is based on the variation of $|\beta_z|$, and the total energy will still be conserved since the electromagnetic wave propagates much more slowly.

In the above results, $s < 0.5\lambda_0$ is assumed throughout which means that the proposed waveguiding structure functions as NRD waveguide. When $s$ increases to $s > 0.5\lambda_0$, the waveguiding structure in Fig. 10 becomes H waveguide, and the results such as slow wave propagation and enhanced energy flow shown in Fig. 12-14 still work.

### 3.2.2 Abnormal guidance and leakage suppression

Usually, all the NRD waveguide and H waveguide components preserve the vertical symmetry so that a general $n = 1$ dependence may be assumed. Therefore, if the modes can leak power, they must do so in the form of $TM_1$ or $TE_1$ mode in the air-filled parallel plate region. Consequently, the condition for leakage can be written as $\beta_z < k_p$, where $k_p$ is the normalized longitudinal wave number of the $TM_1$ or $TE_1$ satisfying $k_p^2 = 1 - (\pi / s')^2$. Given $s = 5$ mm, the waveguiding structure in Fig. 10 works as a NRD waveguide when frequency $f < 30$ GHz. No electromagnetic wave can propagate between the parallel plates because of the cutoff property, thus no leaky wave exits. However, when $f > 30$ GHz, it functions as an H waveguide, therefore, leakage may come into being.

Considering the propagation features of the NRD waveguide and H waveguide with bianisotropic SRR metamaterials, the $|\beta_z|$ of most modes become larger when $f$ increases like the modes in conventional waveguides. However, some higher-order LSM modes in the proposed waveguiding structure may operate dramatically differently. From Eq. (26a),

$$k_z'^2 = \frac{\varepsilon_1}{\varepsilon_2}(\varepsilon_2\mu_2 - \kappa^2 - k_{x1}'^2) - k_y'^2 \tag{35}$$

one can conclude that when $\frac{\varepsilon_1}{\varepsilon_2}(\varepsilon_2\mu_2 - \kappa^2) > 0$, $|k_z|$ will demonstrate a general upward trend as $f$ increase, and may have the chance to get a fall while $\frac{\varepsilon_1}{\varepsilon_2}(\varepsilon_2\mu_2 - \kappa^2) < 0$. The similar trend holds true for $|\beta_z|$.

Fig. 15 presents the abnormal falling behavior of LSM higher-order modes in the proposed NRD waveguide and H waveguide with double negative parameters, and $TM_1$ mode in air filled parallel plate guide. In the region where the dispersion curve of LSM mode is located below the curve of $TM_1$ mode, one expects the leakage. As can be seen, if the falling behavior continues in the H waveguide, leakage will eventually happens. Fortunately, such

higher order modes can propagate only when the parameters are both negative. Moreover, lots of them cannot exit in the H waveguide region since the cutoff of $|\beta_z| = 0$ while $f$ becomes larger.

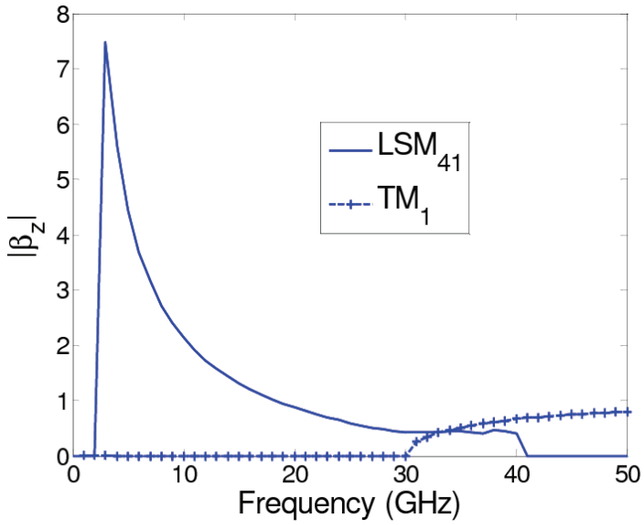


Fig. 15. Abnormal falling behavior of LSM higher modes in the proposed NRD waveguide/H waveguide with double negative parameters ( $\varepsilon_1 = 1$ , $\varepsilon_2 = -3$ , $\mu_2 = -1$ , $\kappa = 1$ , $s = 5$ mm , $q = 5$ mm ) and $TM_1$ mode in air filled parallel plate guide

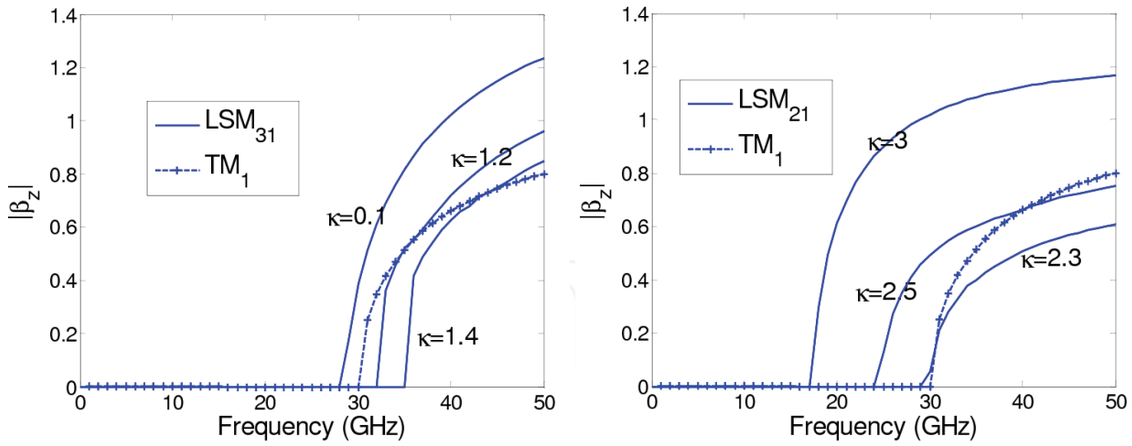


(a) (b)

Fig. 16. Variation of the $|\beta_z|$ versus frequency $f$ for LSM modes in the proposed NRD waveguide/H waveguide ( (a) for double positive metamaterials with $\varepsilon_1 = 1$ , $\varepsilon_2 = 2$ , $\mu_2 = 2.5$ , $\kappa = 0.1,\ 1.2,$ and $1.4$ , $s = 5$ mm , $q = 5$ mm (b) for double negative metamaterials with $\varepsilon_1 = 1$ , $\varepsilon_2 = -3$ , $\mu_2 = -1.5$ , $\kappa = 2.3,\ 2.5,$ and $3$ , $s = 5$ mm , $q = 5$ mm ) and $TM_1$ mode in air filled parallel plate guide

Fig. 16 shows dispersion curve $|\beta_z|$ versus frequency $f$ for LSM modes in proposed H waveguide under the condition $\frac{\varepsilon_1}{\varepsilon_2}(\varepsilon_2\mu_2 - \kappa^2) > 0$. It can be seen in Fig. 16(a), $|\beta_z|$ presents an increase when $f$ becomes lager, but experience a decrease as $\kappa$ turn larger at the same frequency while $\varepsilon_2$ and $\mu_2$ are positive. Therefore, smaller magnetoelectric coupling $\kappa$ will reduce the leakage of the propagating modes. To examine further, from Eq. (21) one knows that positive $\varepsilon_2$ and $\mu_2$ as well as minimum $\kappa$ can exit together in the frequency bands that are far larger than the SRR resonance frequency $\omega_0$, in which the proposed waveguiding structure may exactly works as a H waveguide, thus such reduced leakage scheme can be fulfilled. On the contrary, Fig. 16(b) shows that under the same frequency, $|\beta_z|$ increases when $\kappa$ becomes more significant in the case that $\varepsilon_2$ and $\mu_2$ are both negative. From Eq. (21), one can see that $\varepsilon_2$ and $\mu_2$ have the chance to become both negative when the frequency is little larger than the SRR resonance frequency $\omega_0$. Meanwhile, the magnetoelectric coupling $\kappa$ has the absolute value which can be infinitely large within this frequency band. Therefore, the leakage of guided waves is able to be greatly reduced.

For the more special case when $\varepsilon_2$ and $\mu_2$ are of single negative value, Fig. 17 illustrates that when $\mu_2 > 0$ and $\varepsilon_2 < 0$, $|\beta_z|$ of LSM modes become larger as $\kappa$ increases. Furthermore, the leakage can hardly happen in this case even when $\kappa = 0$, since $\beta_z > k_p$ can be easily satisfied. However, LSE modes will no longer exist under such condition. On the other hand, when $\mu_2 < 0$ and $\varepsilon_2 > 0$, only LSE modes can propagate in the proposed nonradiative dielectric waveguide amd H waveguide, and by choosing proper parameters, the leakage can also be eliminated.

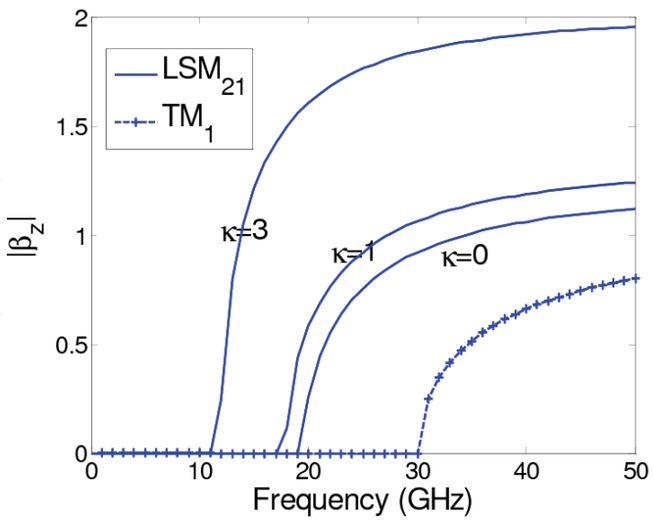


Fig. 17. Variation of the $|\beta_z|$ versus frequency $f$ for LSM modes in proposed NRD waveguide/H waveguide with single negative metamaterials $\varepsilon_1 = 1$, $\varepsilon_2 = -3.5$, $\mu_2 = 1.5$, $\kappa = 0,\ 1,$ and $3$, $s = 5$ mm, $q = 5$ mm and $TM_1$ mode in air filled parallel plate guide

## 4. Metamaterial based multiband frequency selective surfaces

Frequency selective surface (FSS) is a kind of periodically arranged 2D array structure, working like special resonances composed of one or more layers of planar screens and designed to reflect or transmit incident plane waves over specified ranges of frequency. With such unique resonance property, SRR metamaterials are propitious to make frequency selective surfaces (FSSs). Sun et al. [31] investigated a new type of band-pass FSS with metamaterial structures. Baena et al. [32] proposed an isotopic FSS structure based on cubic arrangements of SRR unit, realizing the transmission properties were angle and polarization independent. Marqués et al. [33] illustrated two FSS structures with conventional as well as complementary SRRs and presented ab initio analysis theory.

Typically, the characteristics of an FSS are mainly determined by the shape, size and distribution of the resonant cell. Due to the coupling between the unit cells, the conventional closed element FSSs are often single-band which displays only one dip in the reflection and transmission spectrums. Dual band FSSs, as a breakthrough to the conventional single-band ones, have already realized by fractal elements [34]. And multi-layer structures or complex resonator units are often employed in order to achieve multi-band band-pass or band-stop characteristics of FSS [35,36]. The salient properties of SRR metamaterials have made, and continue to make it possible to fabricate FSSs with enhanced properties that can be rarely obtained by conventional resonance units. Here we demonstrated the multiband FSSs which have several dips in the reflection and transmission spectrums by introducing SRR into the design procedure.

Choosing the FSS structure as shown in Fig. 18, the SRR units are embedded in the dielectric slab with $h = 1$ mm and $\varepsilon_r = 2.2$. The geometric parameters of SRR are $g = 0.4$ mm, $w = 0.5$ mm, $r = 3.9$ mm, $s = 0.6$ mm and repeated in periods of $p = 8$ mm in the $x$ and $y$ direction. It should be noted that such FSS structure will turn into the conventional dual-ring FSS with ring cells when the gaps of the SRR is enclosed.

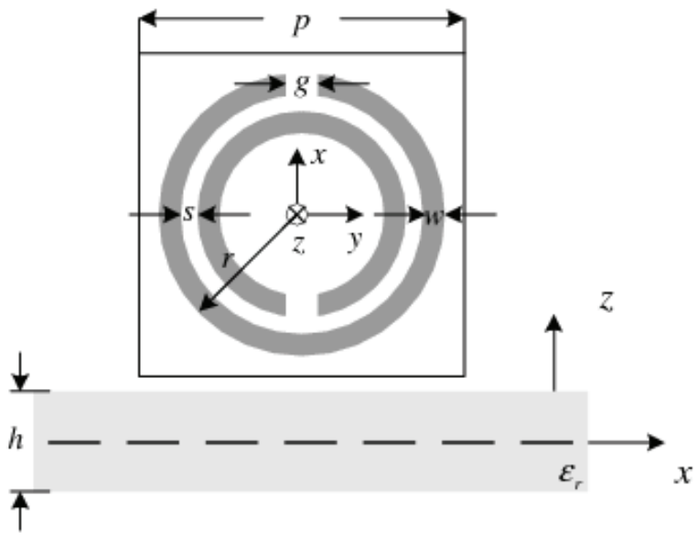


Fig. 18. FSS structure with SRR elements

Fig. 19 shows the resonance response of the FSSs with the SRR and the corresponding dual-ring structure under the normal incident electromagnetic wave. For Fig. 19a ($\theta = 0^\circ$ , $\phi = 0^\circ$), the electromagnetic wave propagates along the $z$-direction with the electric field parallel to the gap bearing sides of the SRR. It can be seen that the transmitted TE-Floquet modes present three resonances when the SRR acts as the resonant cell, while the corresponding FSS with dual-ring structure only demonstrates single resonance. For Fig. 19b ($\theta = 0^\circ$ , $\phi = 90^\circ$), the magnetic field is parallel to the gap bearing sides of SRR. The transmitted TE-Floquet modes represent only one resonant point and the frequency is approximately consistent with the FSS with dual-ring unit structure. Meanwhile, Fig. 19 also indicates that the resonant frequency of the FSS with dual-ring structure is insensitive to $\phi$ at perpendicular incidence. However, the incident angle is crucial for the FSS with the SRR.

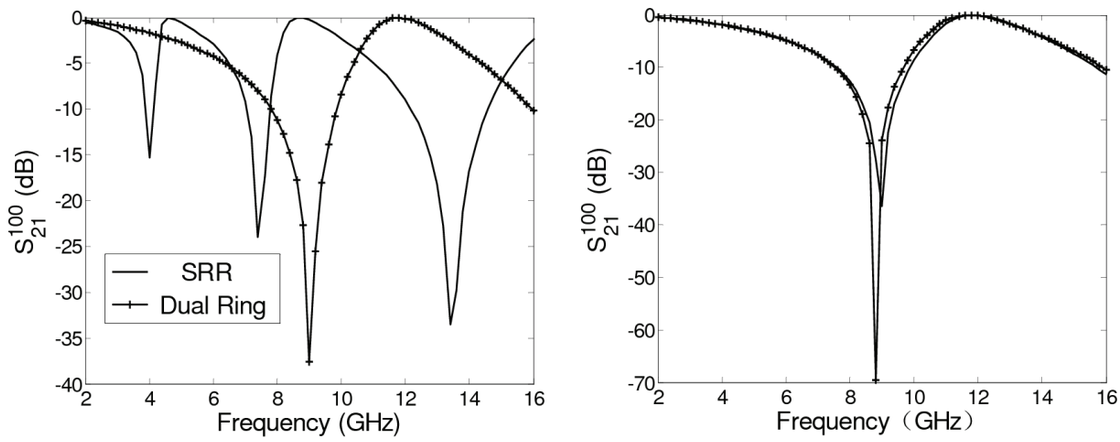


(a) $\theta = 0^\circ$, $\phi = 0^\circ$ (b) $\theta = 0^\circ$, $\phi = 90^\circ$

Fig. 19. Resonance response of the FSS based on SRR and dual-ring structure

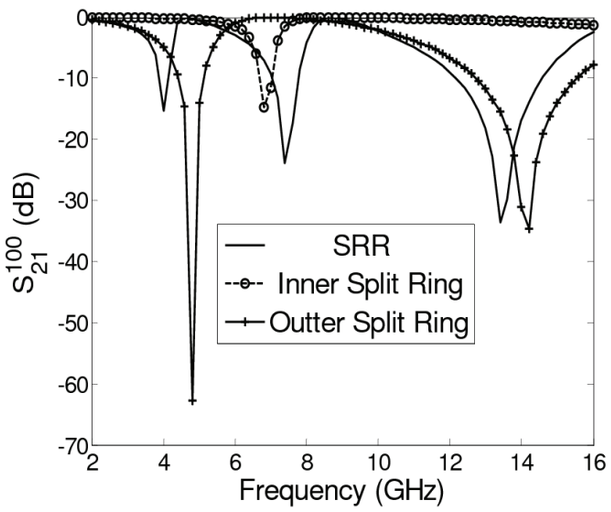


Fig. 20. Resonance response of FSS based on SRR, inner split ring and outer split ring

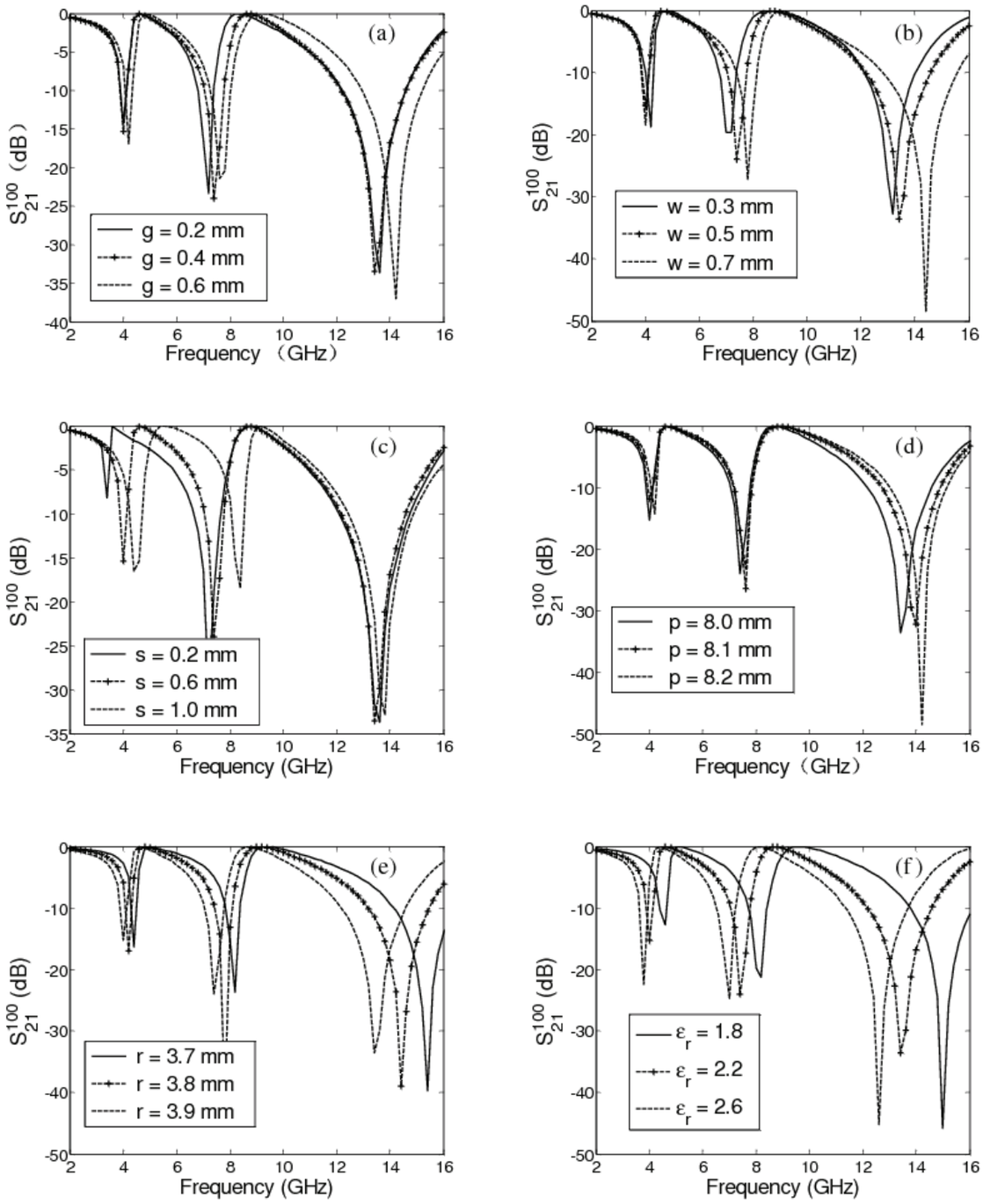


Fig. 21. SRR parameter effects on the resonance properties of the FSSs (a) gap size (b) ring width (c) ring separation (d) unit period (e) outer split ring radius (f) dielectric constant

Fig. 20 displays the resonance response of FSS based on SRR, inner split ring and outer split ring for perpendicular incidence( $\theta = 0^\circ$ , $\phi = 0^\circ$ ). It can be concluded that the three resonant points of the FSS with SRR are engendered by the inner split ring and outer split ring respectively. And the inner split ring determines one point, while the outer split ring determines two. The slight shifts between the resonant frequencies are due to the coupling between the two split rings. Similar results have been illustrated by Kafesaki et al. [37] when studied the transmission properties of left-handed materials, here we provide an alternative numerical techniques by introduce Floquet modes into the analysis of metamaterial based FSSs.

Fig. 21 illustrates the influences of SRR parameter on the resonance properties of the FSSs. By making other parameters stay the same, it can be seen that the increase of gap size *g*, ring width *w*, ring separation *s*, and unit period *p* will lead to the increase of the resonance frequency of the FSS. In contrast, the increase of outer split ring radius *r*, and dielectric constant $\varepsilon_r$ will result in the decrease of the resonance frequency.

Fig. 22 displays the resonance response of the FSS to the electromagnetic wave incident in the z-direction ( $\theta = 0^\circ$ ) from different incidence planes. The orientation of the SRR resonant cell in the FSS to the incident wave changes with the variation of $\phi$ . Namely, the direction of the E-field turns from parallel to the gap to perpendicular to the gap, which makes the electric resonance of the SRR become weaker. As is shown, when $\phi$ increases, the resonance response of the TE-Floquet modes weakens and the three resonant points of the FSS finally transit into only one resonant frequency corresponding to $\phi = 0^\circ$ and $\phi = 90^\circ$, respectively. On the other hand, the resonance response of the TM-Floquet modes experience the opposite variation trend, and the single resonance frequency of the FSS becomes into three resonances due to the gradually enhanced electric resonance.

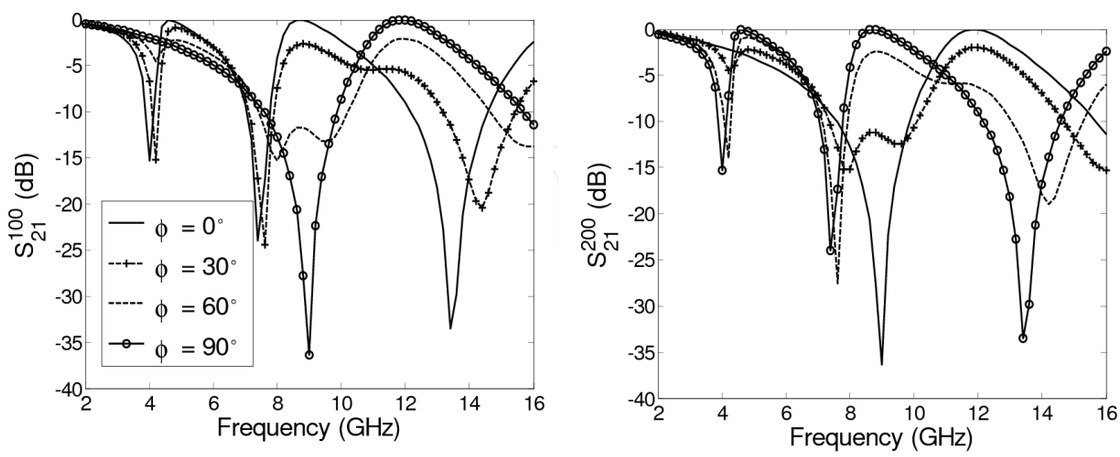


(a) TE-Floquet (b) TM-Floquet

Fig. 22. The FSS resonance response to the electromagnetic wave in the z-direction from different incident planes

Fig. 23(a) shows the transmission property of FSS with the wave incident in the XoZ plane ($\phi = 0^\circ$). As we have demonstrated, the resonance response only occurs in the transmitted Floquet modes with the same polarization as the incident wave from the dominant plane. When $\theta = 0^\circ$, only electric resonance exits. However, the increase of $\theta$ makes H component perpendicularly transmit the SRR, which leads to magnetic resonance. The FSS still keeps three resonances with one point of 7.4 GHz stays the same and the other two points shift slightly. Resonance intensity turns much more complicated because of the combined action of the electric resonance and the magnetic resonance. The resonance point near 4 GHz is of the most significance when $\theta = 30^\circ$, while the resonance points at 7.4 GHz and near 14 GHz are relatively strong when $\theta = 80^\circ$. In addition, the bandwidth of the three resonances turns broader as $\theta$ increases. Fig. 23(b) shows the transmission property FSS with the wave incident in YoZ plane ($\phi = 90^\circ$). In this case, electric resonance weakens a little and the bandwidth decreases when θ increases.

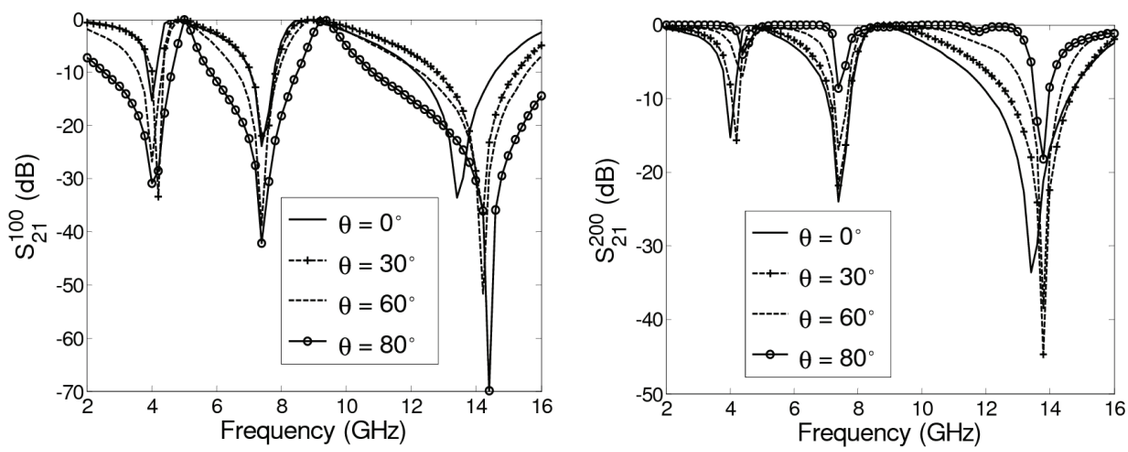


(a) (b)

Fig. 23. The FSS resonance response to the wave incident in (a) the XoZ plane (b) YoZ plane

Fig. 24 and Fig. 25 show the TE- and TM-Floquet mode resonance responses of the FSS for the vertical- and parallel-polarized electromagnetic wave incident in the arbitrary planes, respectively. For any incident angle $\theta$, the resonance response of TE-Floquet mode becomes weaker as $\phi$ increases, while the resonance response for the TM-Floquet mode keeps nearly unchanged as shown in Fig. 20. On the other hand, the TM-Floquet mode resonance response becomes stronger with the increase of $\phi$, while the TE-Floquet mode keeps almost unchanged as shown in Fig. 21. We can concluded that both TE- and TM-Floquet modes will share FSS resonance when either polarized wave incident in the none-dominant plane, however, the transmitted modes with the same polarization as the incident wave are much more sensitive to the incident angle.

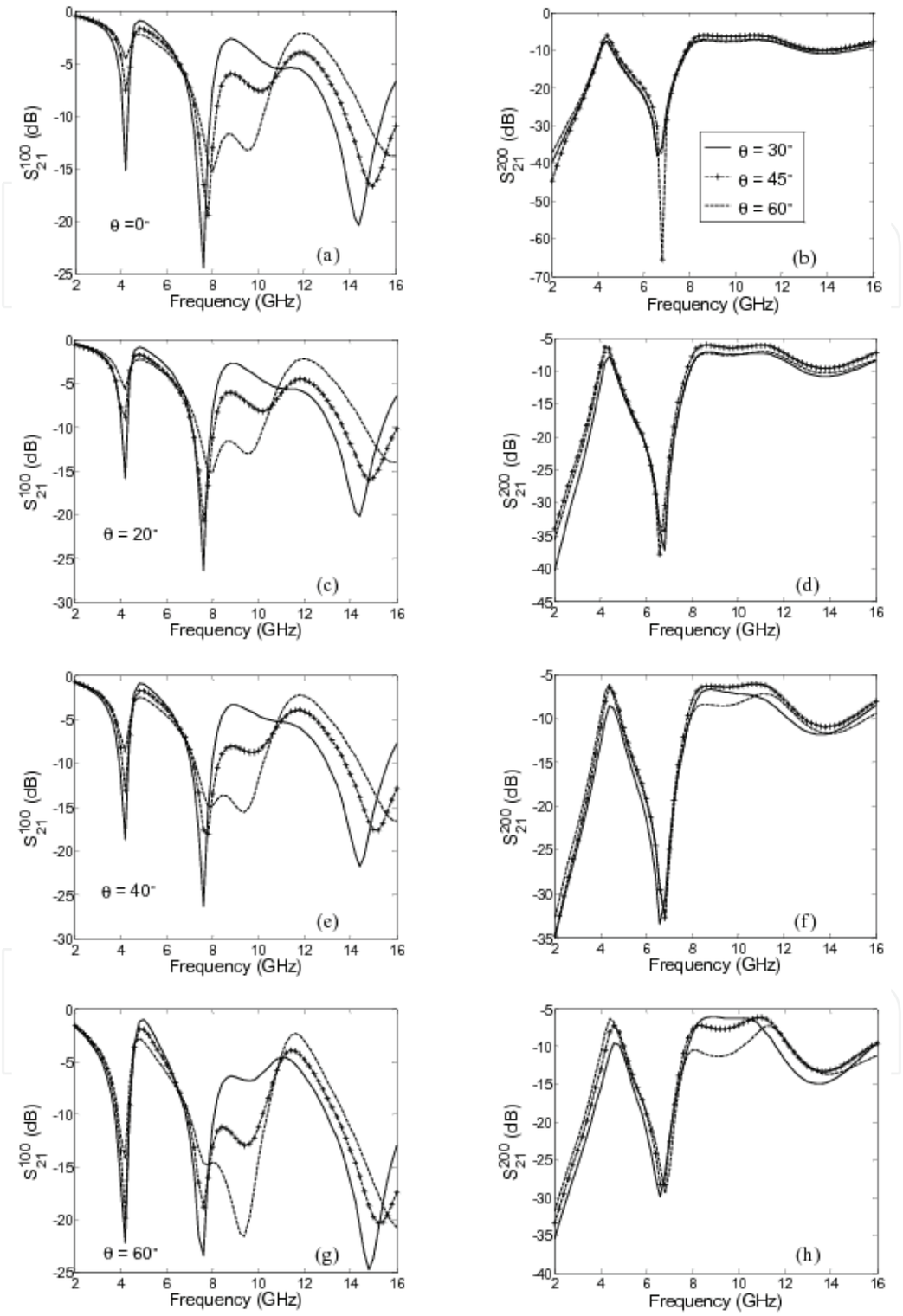


Fig. 24. The resonance responses of the FSS for the vertical-polarized electromagnetic wave in arbitrary plane (a) (c) (e) (g) TE-Floquet modes; (b) (d) (f) (h) TM-Floquet modes

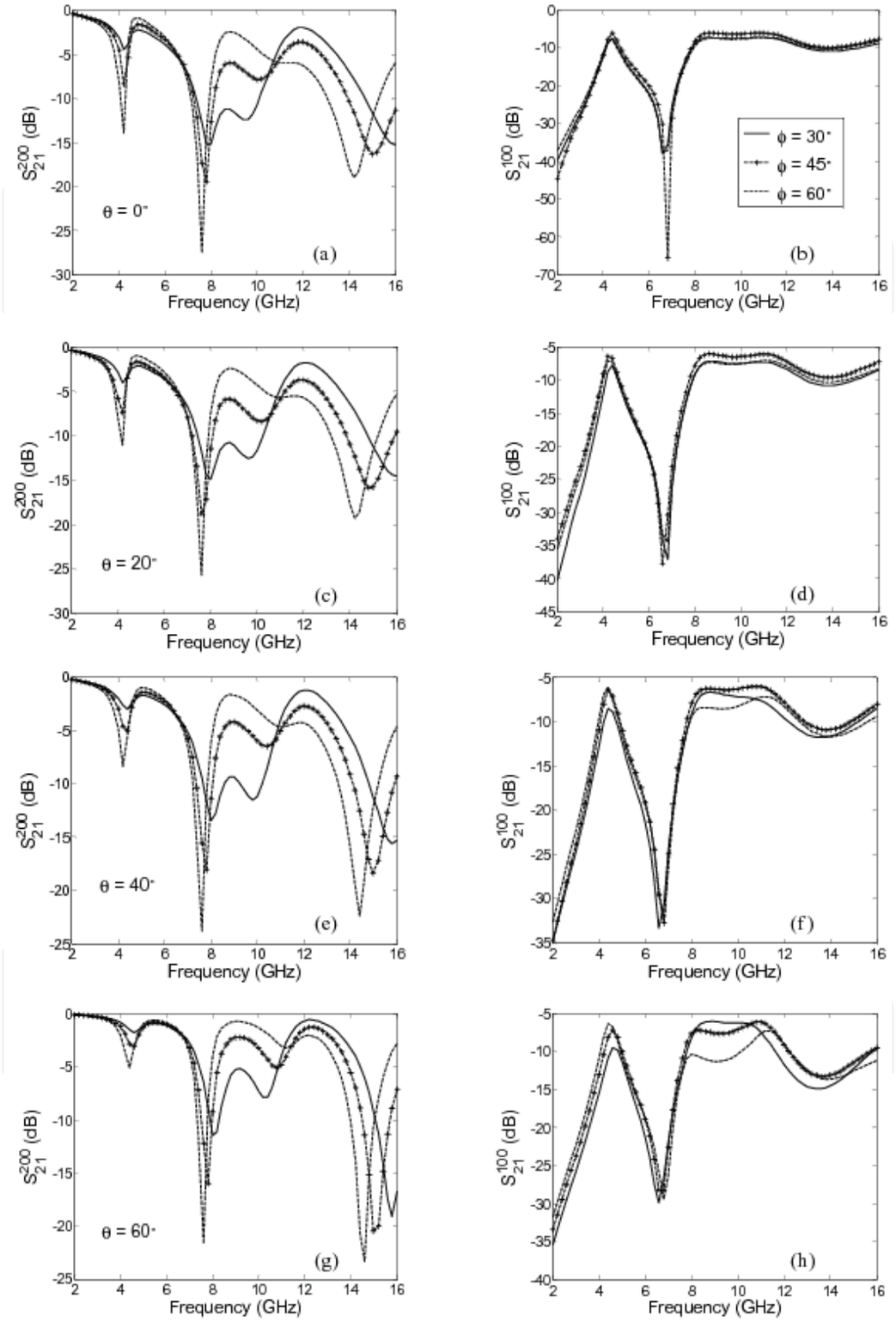


Fig. 25. The resonance responses of the FSS for the parallel-polarized electromagnetic wave in arbitrary plane (a) (c) (e) (g) TM-Floquet modes; (b) (d) (f) (h) TE-Floquet modes

## 5. Conclusion

The nature of electromagnetic waves in metamaterials and metamaterial-inspired configurations has been studied in this chapter [38-42]. First, causality in the resonance behavior of metamaterials has been developed. Both a rigorous full wave analysis and Floquet mode theory have been employed to examine the various electromagnetic fields effects on metamaterials. Second, propagation features of metamaterial waveguiding structures have been intensively explored. It is shown that different dispersion properties, such as non-cutoff frequency mode propagation and enhanced bandwidth of single mode operation, have been impart to metamaterial based parallel plate waveguide and rectangular waveguide. Meanwhile, slow wave propagation, enhanced energy flow, abnormal higher-order modes, as well as leakage suppression of LSM and LSE modes are illustrated in the NRD waveguide and H waveguide with bianisotropic SRR metamsterials. Finally, multiband transmission property of FSSs with SRR unit cells is illustrated. As is shown, such multi-band spectrum is closely related to the SRR parameters as well as incident wave.

It is worth noting that the electromagnetic responses of SRR metamaterials are in fact much more complicated for practical use. Therefore, restrictive conditions, such as the absence of losses, certain direction of the incident wave, are assumed throughout the full wave analysis. However, we here consider the macroscopical effects of material parameters of the media, providing alternative means of characterizing the SRR metamaterials and its inspired waveguding structures. In addition, the SRR element spacing of the metamaterials are usually small compared to the resonance wavelength, and only the modes of $p = 0$ and $q = 0$ can propagate in the distant transmitted fields. Therefore, resonance behavior of SRR metamaterials and their transmission properties have been examined only through the dominant TE- and TM-Floquet modes in the Floquet mode analysis.

## 6. Acknowledgement

This work was supported in part by National Natural Science Foundation of China (Grant No. 60771040) and in part by State Key Laboratory Foundation (Grant No. 9140C0704060804). The work of Dr. Rui Yang was supported by Newton International Fellowship.

## 7. Reference

[1] V. G. Veselago, *Sov. Phys. Usp.*, 10 (1968) 509.
[2] J. B. Pendry, A. J. Holden, W. J. Stewart, and I. Youngs, *Phys. Rev. Lett.*, 76 (1996) 4773.
[3] R. A. Shelby, Smith D. R., and Schultz S., *Science*, 292 (2001) 77.
[4] R.Marqués, F. Medina, and R.Rafii-El-Idrissi, *Phys. Rev. B*, 65 (2002) 144440.
[5] D. R. Smith, J. Gollub, J. J. Mock, W. J. Padilla, and D. Schurig, *J. Appl. Phys.*, 100 (2006) 024507.
[6] D. R. Smith, D. Schurig, and J. J. Mock, *Phys. Rev. E*, 74 (2006) 036604.
[7] V. V. Varadan, and A. R. Tellakula, *J. Appl. Phys.*, 100 (2006) 034910.

[8] K. Aydin, K. Guven, N. Katsarakis, C. M. Soukoulis, and E. Ozbay, *Opt. Exp.*, 12 (2004) 5896.
[9] P. Gay-Balmaz, and O. J. F. Martin, *J. Appl. Phys.*, 92 (2002) 2929.
[10] N. Katsarakis, T. Koschny, M. Kafesaki, E. N. Economou, and C. M. Soukoulis, *Appl. Phys. Lett.*, 84 (2004) 2943.
[11] J. B. Pendry, *Phys Rev Lett.*, 85 (2000) 3966.
[12] F. Martín, F. Falcone, J. Bonache, R. Marqués, and M. Scrolla, *Appl. Phys. Lett.*, 83 (2003) 4652.
[13] F. Aznar, J. Bonache, and F. Martín, *Appl. Phys. Lett.*, 92 (2008) 043512.
[14] R. W. Ziolkowski, *IEEE Trans. Antennas Propagat.*, 45 (2003) 656.
[15] K. Aydin, I. Bulu, K. Guven, M. Kafesaki, C. M. Soukoulis, and E. Ozbay, *New J. Phys.*, 7 (2005)168.
[16] T. F. Gundogdu, I. Tsiapa, A. Kostopoulos, G. Konstantinidis, N. Katsarakis, R. S. Penciu, M. Kafesaki, E. N. Economou, Th. Koschny, and C. M. Soukoulis, *Appl. Phys. Lett.*, 89 (2006) 084103.
[17] C. R. Simovski, and S. A. Tretyakov, *Phys. Rev. B*, 75 (2007) 195111.
[18] C. R. Simovski, *Metamaterials*, 1 (2007) 62.
[19] N. Amitay, and V. Galindo, *Bell Syst. Tech. J.*, 47 (1968) 1903.
[20] C. C. Chen, *IEEE Trans. Microwave Theory Tech.*, 18 (1970) 627.
[21] C Krowne., *IEEE Trans. Antennas Propag.*, 32 (1984) 1224.
[22] A. Alú and N. Engheta, *IEEE Trans. Microw. Theory Tech.*, 52, (2004) 199.
[23] B.-I. Wu, T. M. Grzegorczyk, Y. Zhang, and J. A. Kong, *J. Appl. Phys.*, 93, (2003) 9386.
[24] Y. S. Xu, *Microwave Opt. Technol. Lett.*, 41, (2004) 426.
[25] I. V. Shadrivov, A. A. Sukhorukov, and Y. S. Kivshar, *Phys. Rev. E*, 67, (2003) 057602.
[26] S. Hrabar, J. Bartolic, Z. Sipus, *IEEE Trans. Antennas Propag.*, 53, (2005) 110.
[27] A. L. Topa, C. R. Paiva, and A. M. Barbosa, *Microwave Opt. Technol. Lett.*, 47, (2005) 185.
[28] P. Yang, D. Lee, and K. Wu, *Microwave Opt. Technol. Lett.*, 45, (2005) 207.
[29] P. Baccarelli, P. Burghignoli, F. Frezza, A. Galli, P. Lampariello, and S. Paulotto, *Microwave Opt. Technol. Lett.*, 48, (2006) 2557.
[30] S. A. Tretyakov, *J. Electromagn. Wave Applic.*, 12, (1998) 821.
[31] Q. H. Sun, Q. Cheng, H. S. Xu, B. Zhou, and T. J. Cui, *META08'Nanjing*, (2008) 267.
[32] J. D. Baena, L. Jelinek, R. Marqués, J. J. Mock, J. Gollub, and D. R. Smith, *Appl. Phys. Lett.*, 91, (2007) 191105.
[33] R. Marqués, J. D. Baena, M. Beruete, F. Falcone, T. Lopetegi, M. Sorolla, F. Martín, and J. Garcia, *J. Opt. A: Pure Appl. Opt.*, 7, (2005) 38.
[34] J. Romen, and Y. Rahmat-Samii, Electron. Lett., 35, (1999) 702.
[35] R. Mittra, C. H. Chan, and T. Cwik, Proc. IEEE, 76, (1998) 1593.
[36] B. A. Munk, New York: Wiley, 2000.
[37] M. Kafesaki, Th. Kosohny, R. S. Penciu, T. F. Gundogdu, E. N. Economou, and C. M. Soukoulis, *J. Opt. A: Pure Appl. Opt.*, 7, (2005) 12.
[38] R. Yang, Y. J. Xie, X. F. Li, Y. Y. Wang, J. Jiang, Europhys. Lett., 84, (2008), 34001.

[39] R. Yang, Y. J. Xie, X. D. Yang, R. Wang, B. T. Chen, Opt. Express, 17, (2009), 6101.
[40] R. Yang, Y. J. Xie, J. Jiang, Y. F. Gong, IEEE Antennas Wireless Propag. Lett., 7, (2008), 481.
[41] R. Yang, Y. J. Xie, X. F. Li, J. Jiang, Infrared Phys. Techn., 51, (2008), 555.
[42] R. Yang, Y. J. Xie, META08'Nanjing, Invited Paper.


**Wave Propagation in Materials for Modern Applications**

Edited by Andrey Petrin

ISBN 978-953-7619-65-7
Hard cover, 526 pages
**Publisher** InTech
**Published online** 01, January, 2010
**Published in print edition** January, 2010

In the recent decades, there has been a growing interest in micro- and nanotechnology. The advances in nanotechnology give rise to new applications and new types of materials with unique electromagnetic and mechanical properties. This book is devoted to the modern methods in electrodynamics and acoustics, which have been developed to describe wave propagation in these modern materials and nanodevices. The book consists of original works of leading scientists in the field of wave propagation who produced new theoretical and experimental methods in the research field and obtained new and important results. The first part of the book consists of chapters with general mathematical methods and approaches to the problem of wave propagation. A special attention is attracted to the advanced numerical methods fruitfully applied in the field of wave propagation. The second part of the book is devoted to the problems of wave propagation in newly developed metamaterials, micro- and nanostructures and porous media. In this part the interested reader will find important and fundamental results on electromagnetic wave propagation in media with negative refraction index and electromagnetic imaging in devices based on the materials. The third part of the book is devoted to the problems of wave propagation in elastic and piezoelectric media. In the fourth part, the works on the problems of wave propagation in plasma are collected. The fifth, sixth and seventh parts are devoted to the problems of wave propagation in media with chemical reactions, in nonlinear and disperse media, respectively. And finally, in the eighth part of the book some experimental methods in wave propagations are considered. It is necessary to emphasize that this book is not a textbook. It is important that the results combined in it are taken “from the desks of researchers“. Therefore, I am sure that in this book the interested and actively working readers (scientists, engineers and students) will find many interesting results and new ideas.

University Campus STeP Ri
Slavka Krautzeka 83/A
51000 Rijeka, Croatia
Phone: +385 (51) 770 447
Fax: +385 (51) 686 166
www.intechopen.com

Unit 405, Office Block, Hotel Equatorial Shanghai
No.65, Yan An Road (West), Shanghai, 200040, China
中国上海市延安西路65号上海国际贵都大饭店办公楼405单元
Phone: +86-21-62489820
Fax: +86-21-62489821



IntechOpen

IntechOpen